OPEN ACCESS
Unmanned Systems (2026)

DOI: 10.1142/S2301385026500123

Unmanned Systems
https://www.worldscientific.com/worldscinet/us

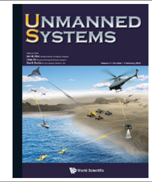

Multitasking Capabilities of an Autonomous quad-Arm Mobile Manipulator (qAMM) for Smart City Operations

Ravinesh Chand [*,†,‡], Sandeep A. Kumar [†], Bibhya Sharma [†], Ronal P. Chand [*]

[*] School of Mathematical & Computing Sciences,
Fiji National University, Fiji

[†] School of Information Technology,
Engineering, Mathematics & Physics,
The University of the South Pacific, Fiji

Additional robotic arms on a mobile manipulator invariably enhance its multi-tasking capabilities and offer greater flexibility in performing multiple complex operations. This paper presents a four-arm or quad-arm car-like mobile manipulator (qAMM) that can address the issue of labor shortage in emerging smart city operations that require multi-tasking such as garbage collection, construction, maintenance, and cleaning. Lyapunov-based acceleration controllers are derived and utilized to solve the proposed mobile manipulator's motion planning and control problem. First, a dual-step algorithm is used to move the car-like base in an obstacle-ridden environment from an initial position to its pseudo-target and, second, maneuver the four end-effectors to their designated targets and enable qAMM to perform multiple tasks through the synchronous and asynchronous motion of its revolute links. Furthermore, by using the Direct Method of Lyapunov and LaSalle's invariance principle, stability and convergence analyses of the four-arm car-like system have been proved. Finally, the effectiveness of the proposed approach and qAMM's acceleration-based motion controllers is verified by computer simulations.

Keywords: Multiple tasks; synchronous; asynchronous; pseudo-target; mobile manipulator; end-effector.

US

1. Introduction

The emergence of advanced technology tools has helped create new products and multi-functional devices in the modern era. Technology contributes to innovation in the industrial sector, leading to high productivity and efficiency. The expectations from dynamic industrial settings are widespread which has resulted in increased adoption of robotic automation in manufacturing sectors. Robots are programmed to make precise movements and perform multiple tasks with repeatability, resulting in increased productivity. As such, autonomous mechanical systems have emerged as one of the most rapidly growing disciplines of scientific research, contributing to an increased deployment of automated mobile robots in various research as well as industrial and smart city environments [1–3]. Advances in research on mobile robots with a high degree of autonomy are possible, on the one hand, because of increased accessibility of cost-effective robotics technology and, on the other hand, because of a wide range of applications. Due to their high capabilities, mobile robots can replace humans in diverse applications such as surveillance, emergency rescue operations, construction, part transportation in factories, material handling in manufacturing, household cleaning, medical care, volcano inspection, and planet exploration, to mention some [4, 5].

Various mobile robots have been designed over the years to suit the demands and requirements of the intended application, which, therefore, can be categorized according to the environment in which they work and their mobility.

Received 12 May 2024; Revised 30 January 2025; Accepted 1 February 2025; Published 26 May 2025. This paper was recommended for publication in its revised form by editorial board member, Bayu Jayawardhana.
Email Address: ‡*ravinesh.c@fnu.ac.fj*
‡ Corresponding author.

Some of the major categories of mobile mechanical systems addressed in the literature include Autonomous Underwater Vehicles (AUV), Unmanned Aerial Vehicles (UAV) like drones, and Unmanned Ground Vehicles (UGV) in the form of legged robots as humanoids, as well as wheeled robots such as Segway, wheelchairs, tractor-trailer systems, and car-like robots. Considering their practical applications in industry, communications, transportation, and more recently in smart city operations, car-like robots are known to be the most predominant amongst wheeled robots [6, 7]. Low maintenance costs, easy manufacturing, ability to maneuver at high speed, ability to carry heavy loads, and proper suspension systems are the main advantages of car-like robots [7]. One such prominent car-like robot is a car-like mobile manipulator, a mechanical system usually comprising a robotic arm mounted on a moving car-like wheeled platform. Integrating a robotic manipulator arm into a mobile platform provides a mobile manipulator with specific maneuverability within a workspace that anchored manipulators cannot. Moreover, car-like manipulators can be used as assistive co-workers to help increase the accuracy of industrial processes and safety in the workspace. For instance, autonomous car-like manipulators were deployed in the automotive industry for automotive assembly by assisting workers in transporting heavy vehicular parts at different stages along the assembly line, thus increasing productivity and quality while simultaneously reducing fatigue levels among workers [8]. As a result, vital industrial operations like intelligent transportation and material handling have become more flexible and productive due to the industrial application of car-like mobile manipulators [7].

Esmaeilian *et al.* [2] stated that the current demand for improving workflows in urban areas has paved the way for car-like manipulators to be utilized as smart urban transportation systems to perform time-consuming service tasks such as removing cigarette butts, chewing gum, and weeds from flower gardens and pathways. The implementation of smart city robots has created new opportunities for managing city operations efficiently and which are economically feasible while improving working conditions and ergonomics for the operators involved [8]. Furthermore, the added feature of robotic arms installed on autonomous intelligent vehicles is advantageous and ideal for repetitive and consistent operations that require high accuracy. Despite such significant advantages and vast applications, research has centered mainly around single-arm [4, 7], and dual-arm car-like manipulators [9–11]. In this research, the task-performing capabilities of a single-arm and dual-arm mobile manipulator are further extended to include four revolute arms (quad-arms) mounted on a car-like platform in the form of an intelligent vehicle system for improved multi-tasking capabilities.

The goal of implementing a robot with four arms that can perform multiple and complex manipulation tasks using the Artificial Potential Field (APF) method is still a challenging research topic. However, work is continuing because of the commercial potential for automating tasks requiring tiresome multi-tasking operations. The additional complexity of four-arm manipulation provides many challenges that may be absent in the single or dual-arm manipulator framework, implying that four-arm manipulation requires more advanced planning and viable control approaches [1]. The correlation between the individual robotic arms of such mechanical systems is critical to attaining desired maneuverability. If the synchronization between the arms is poor, the stability and performance of the system will decrease accordingly. With regards to movement and execution of assigned tasks, a four-arm mobile manipulator can be used for performing multiple tasks, including pick-and-place and loading and unloading of objects. While performing tasks, the arms can either operate synchronously, for example, with all arms simultaneously picking the same object and placing it at the destination together, or asynchronously, where all the arms of the robot pick different things and perform entirely different tasks. Therefore, four-arm robotic systems demand more explicit computer codes and control algorithms to successfully navigate targets, collision avoidance, and task deployment.

In smart city environments, a challenging problem remains on how to control the motion of an autonomous mobile manipulator and improve its effectiveness by guiding it to accomplish assigned tasks efficiently in a constrained workspace. Motion control algorithms help facilitate an autonomous mobile manipulator's navigation in performing defined tasks. Numerous motion control approaches, which generally fall under classic and heuristic-based methods, have been studied and utilized to design appropriate motion controllers for successfully executing assigned robotic tasks [12]. In their review of classical and heuristic-based navigation, Atyabi *et al.* [12] disclosed that heuristic-based algorithms generally have a slow convergence rate and do not guarantee an immediate solution in comparison to classical approaches. The APF method, which belongs to the classical approach, provides simple and effective motion planners and involves a robot moving under the influence of potential fields determined by obstacles and the target configuration. Several practical APF methods have recently been developed for motion control of single-arm, and dual-arm car-like manipulators [9]. The Lyapunov-based Control Scheme (LbCS) is an APF method that utilizes a carefully constructed Lyapunov function, which acts as an energy function, for designing the motion controllers of robotic systems [12]. As a result, LbCS will be utilized to solve the proposed four-arm vehicle system's motion planning and control problem.

This research is inspired by the lack of attention given by researchers to a four-arm car-like mobile manipulator to address labor shortage problems in multi-tasking operations of emerging smart cities and industrial environments. This paper presents the kinematic design and adoption of an autonomous car-like mobile manipulator with four revolute arms (qAMM). It provides solutions to its findpath problem with the requirement that the car-like system navigates to assigned targets in an obstacle-ridden environment. To the authors' knowledge, having four revolute arms installed on the mobile base is ideal for performing assigned tasks, as opposed to numerous arms where the rest of the arms which are not in use have to be made redundant to avoid operational complexities like collision avoidance amongst the arms, model design, restrictions in arm installation and system stability issues [13]. Furthermore, the switched nonlinear, stabilizing, time-invariant, and continuous acceleration-based controllers derived using the method of LbCS will ensure that the car-like mobile platform and the four revolute arm end-effectors successfully maneuver from their initial to final configurations.

The structure of the paper is organized as follows to guide the reader through the key concepts and findings. In Sec. 2, a brief description of the Lyapunov-based Control Scheme is provided. Then, the system modeling and kinematic analysis of qAMM are provided in Sec. 3. qAMM's targets and trajectory control are presented in Sec. 4, and the acceleration-based controllers are designed in Sec. 5. Next, Sec. 6 analyzes the system's stability, while Sec. 7 provides the convergence analysis. Then, Sec. 8 presents the simulation results, followed by a discussion and conclusion in Secs. 9 and 10, respectively.

1.1. *Literature review*

Mobile car-like mechanical system, being well-researched in literature, has seen remarkable developments in the past decades, but the added complexity of multiple robotic arms mounted on such a system has continuously provided challenges to researchers. The complexities and challenges have led to increased interest in car-like mobile manipulators such as no-arm, single-arm, dual-arm, and multiple-arm manipulators. As a result of this growing interest, several control algorithms have been proposed to address the motion planning and control problem of car-like manipulators.

Mobile manipulators are designed for motion which must be planned and controlled carefully to achieve the desired result. Therefore, the ability of a mobile manipulator to execute the efficient movement and collision-free trajectories within its work environment is essential to its success [5]. The pioneering work on motion control of mobile manipulators was carried out in 1998 by Seraji [14], which is now considered a landmark result in the literature [4]. Seraji's milestone result was established on the development of a set of differential kinematic equations commanding the motion of a car-like mobile manipulator by effectively combining the nonholonomic base constraints, the desired end-effector motion, and the redundancy resolution goals. The work done by Seraji attracted the attention of many researchers and has resulted in the design and development of various types of mobile manipulators.

Technological advances have further enhanced mobile manipulators' capabilities to perform complex tasks that were previously difficult and unsafe for human workers. However, obtaining feasible solutions to the motion planning and control problem while introducing a new mobile manipulator is challenging yet vital for its coordinated, controlled, and collision-free movements in the workspace. Over the years, numerous control algorithms, which generally fall under classic and heuristic-based approaches, have been developed to solve mobile manipulators' motion planning. Although found to be effective as a result of a minimal computation, the classic methods take more time to generate a feasible collision-free path, and the mechanical systems tend to get trapped when there is a cancellation of equal magnitudes of attractive and repulsive forces [15]. To improve the efficiency of classic methods, Artificial Potential Field (APF) methods such as the modified APF [6] and improved APF [16] have been utilized to achieve mobile robot navigation in obstacle-ridden environments. LbCS, which belongs to the classical APF approach, has been used in studies such as [5, 7] for solving the motion planning and control problem of car-like robotic systems and addressing the stability issues of various nonlinear systems [4, 12]. Vanualailai *et al.* [17] in 2008 employed a nonholonomic car-like vehicle to generate artificial potential fields with a collision-free trajectory of the system state and asymptotic stability properties using the Lyapunov method.

The controllers derived using LbCS easily account for system singularities and constraints and have been successfully utilized to achieve stable motion by constructing attractive and repulsive potential fields [17]. A review of recent research works on car-like manipulators comprising robotic arms reveals that there has been a paradigm shift to using generalized n-links for single robotic arms mounted on car-like vehicles [5, 7]. In 2012, Sharma *et al.* [15] used the Lyapunov method to generate continuous nonlinear controllers that, to some extent, simultaneously solved the multi-task problem of steering and navigation of a nonholonomic car-like mobile robot comprising an n-link revolute robotic arm mounted on the mid-front axle of the platform. Later, in 2018, Sharma *et al.* [4] established a set of decentralized acceleration-based control laws using LbCS to solve the problem of rigid control of a team of n-link doubly nonholonomic car-like manipulators, facilitated by moving ghost targets, operating within a constrained environment.

More recently, in 2021, Chand *et al.* [7] used LbCS to solve a car-like mobile robot's motion planning and control problem with an extendible prismatic arm comprising $n \in N$ links. In addition, Prasad *et al.* [5] presented a new 2-Step algorithm for the motion planning and control problem of a three-dimensional articulated mobile manipulator comprising a car-like mobile platform and an n-link articulated arm using the LbCS and Minimum Distance Technique for obstacle avoidance. Along with collision avoidance of fixed obstacles, the car-like robot was subjected to kinematic, navigation, and stability constraints. Despite the complicated task of motion planning and stability of nonholonomic car-like vehicles, the authors of [4, 5, 15] managed to achieve stability for nonholonomic systems using continuous acceleration control laws derived from LbCS for posture stabilization of car-like mobile robots within a constrained workspace. The studies demonstrated collision-free maneuvers and multi-tasking problems of car-like robots considering kinodynamic constraints.

While most research works on mobile manipulators concentrated on singular planar arms, a few have considered dual planar arms mounted on car-like robots. In 1995, Agrawal *et al.* [11] demonstrated a space application using an anchored dual-arm manipulator with both arms functioning asynchronously, where one of the arms was required to perform a specific task while the other performed the motions necessary to keep the base fixed at a position. In their study, algorithm-based position kinematics equations and an iterative search procedure were used; however, the major problem was avoiding the singularities. Eberle *et al.* [18] in 2020 studied the synchronization motion of a dual-arm Baxter robot to collaborate and coordinate with other robots using the Anticipating Synchronization (AS) control scheme. Feedback delays, controlling and predicting other robots' movements, and anticipating arm movements while attempting synchronous control were some of the challenges encountered in this study.

Although single-arm and dual-arm robots can be advantageous for specific tasks, a multiple-arm system gives users agility due to human-like control over their environment, especially in dull, dirty, and dangerous applications. Early multiple-arm mechanical systems were teleoperated, with the operator directly controlling the trajectory and sequence of movements of the robot [10]. However, the introduction of more autonomous systems in the late 1990s saw increased research interest in finding feasible methods for motion planning of mobile multiple-arm systems. For example, Takahama *et al.* in 2004 [19] attempted a complicated pick-and-place motion planning for synchronous multiple-arm mobile manipulators, which required picking a book and placing it on a shelf using the inverse kinematics algorithm. Unfortunately, omni-wheels' slippage led to difficulties in controlling the robot's position, which could have been avoided if, in their research, hybrid algorithms or improved classical approaches that could have accounted for the omnidirectional motion were utilized instead [19].

More recently, companies have adopted automation and robotic systems to tackle operational challenges, mainly accelerating smart city initiatives such as autonomous garbage detection and collection. In their concept paper, Esmaeilian *et al.* [2] reported a growing movement towards introducing car-like robots for rubbish-picking tasks in polluted environments. Abbasi *et al.* [3] studied the visual analytic system in 2018 using the Deep Neural Network (DNN) algorithm to learn the complex patterns required for smart city applications like sidewalk pavement sweeping and rubbish detection. The experimental results demonstrated the proposed algorithm's effectiveness in performing complex inspection and service tasks required for smart city operations. In 2019, West *et al.* [20] combined a mobile manipulator, namely a Clearpath Husky robot with a Universal Robots UR5 robot arm, and used simulated 2D Lidar data with a Simultaneous Localization and Mapping (SLAM) algorithm to perform a variety of valuable tasks including clearing debris in contaminated environments. Samonte *et al.* [21] in 2021 developed and tested a solar-powered smart bin system with a car-like robotic garbage collector named e-TapOn. The proposed automated guided car (AGV) utilized the Raspberry Pi and Arduino UNO microcontrollers integrated with ultrasonic, height, and color sensors in a web-based system to automatically recognize polyethylene terephthalate or PET bottles in food and beverage packaging. However, the accuracy of gathering data could have been increased by using more appropriate smart sensors.

This literature search reveals that extensive research on motion planning and control algorithms of car-like robots has been done, where the robots have single-arm, dual-arm, or no arms. However, advancement in the field of four-arm car-like mobile robots to address real-life problems applicable to smart city environments is still work in progress. This research addresses the motion control problem of a four-arm mobile manipulator (qAMM) to perform multiple tasks synchronously or asynchronously as required using the method of LbCS.

1.2. *Main contributions*

The main contributions of this paper are

(1) *design of a four-arm car-like robot (qAMM) whereby each articulated arm, comprising two revolute links and an end-effector, is mounted on the ends of the front and*

rear axles of a car-like mobile base. The qAMM has better multitasking capabilities than the single-arm mobile systems utilizing APF methods [5, 7] or the dual-arm systems utilized for collision-avoidance using a hybrid control method [1], position kinematics algorithm [11] and particle swarm optimization (PSO) [22], where the robots were only able to perform limited tasks at a time. While only a handful of researchers have studied motion planning and control of four-arm car-like robots [19], this paper contributes to the literature on four-arm mechanical systems. With its articulated arms, this mobile manipulator can perform multiple assigned tasks and offers an ideal solution for addressing labor shortages in various smart city applications such as garbage collection, construction, maintenance, and cleaning.

(2) *mathematical integration of the LbCS with a dual-step target attraction algorithm for switch movement of the mobile car-like base and the four revolute arms of qAMM.* While the motion planning and control problem of an autonomous four-arm car-like vehicle has been addressed using different control algorithms [19], LbCS as an approach has not been considered yet. To the best of the authors' knowledge, this is the first time such continuous acceleration-based controllers are designed using LbCS to solve the motion planning and control problem of a four-arm car-like robot in an environment cluttered with fixed obstacles. The acceleration controllers are continuous compared to non-continuous heuristic controllers [22], and assure smooth trajectory and motion compared to velocity-based systems, which may lead to erratic movement due to sudden changes in angular velocities [7]. Furthermore, the motion controllers derived in this study can be applied to address motion control problems in other appropriate autonomous transportation systems of emerging smart cities.

(3) *synchronous and asynchronous arm movements of qAMM for performing multiple tasks.* By assigning targets appropriately to the end-effectors, the revolute arms can be subjected to operate in coordination and perform a collective task synchronously or entirely different tasks asynchronously. This unique synchronization behavior of qAMM's four arms makes it ideal for performing various tasks efficiently such as assembly of parts, pick-and-place, rubbish collection, maintenance, and cleaning. In contrast, the car-like mobile manipulators reported in the literature faced difficulties in attempting to perform tasks asynchronously [11] and synchronously [19].

2. Lyapunov-Based Control Scheme (LbCS)

Motion controllers play a pivotal role in guiding the precise movements of car-like robotic systems, and LbCS stands out as a highly effective approach in achieving stability and optimized performance. The LbCS has been successfully utilized to solve problems that arise from motion planning and control of various robotic applications. It addresses autonomous navigational issues such as obstacle avoidance, parking maneuverability, and point and posture stabilization typically encountered in mechanical system design. It also treats the kinodynamic constraints tagged to newly designed autonomous mechanical systems.

The LbCS is a motion control scheme used to provide nonlinear control design solutions for problems that arise from robotic systems required to interact with and manipulate their environments. In this approach, artificial potential field functions in the form of target attraction functions are developed, which guarantee the convergence of the planar robot to its designated targets. For obstacle avoidance, we assign LbCS a strategy inspired by Sharma *et al.* in [15] to develop a repulsive potential field function that fundamentally is a ratio that encodes the obstacle avoidance function into its denominator while the numerator consists of a tuning parameter. This ratio, called the repulsive potential field function, ensures the avoidance of an obstacle. The control scheme requires the summation of all the attractive and repulsive potential field functions, commonly referred to as a Lyapunov function. The attractive potential field functions will attach attractive fields to the targets for attraction and goal convergence. In contrast, the repulsive potential field functions will establish repulsive fields to the obstacles for successful avoidance. The system restrictions and singularities are developed as artificial obstacle avoidance functions which are part of the total potential. These restriction functions for qAMM include velocities, steering angles and revolute link angle limitations. Moreover, the LbCS approach is quite flexible and accommodating in nature as it can address disk, elliptic, rectangular and rod-shaped obstacles [4, 5]. The scheme requires the differentiation of the Lyapunov function to derive the continuous motion control laws that govern an autonomous mechanical system.

In Fig. 1, the Lyapunov function's 3D visualization and contour plot are shown. A robot, initially at (10,10) navigates to its assigned target at (100,100) while avoiding two stationary obstacles located at (50,30) and (50,80).

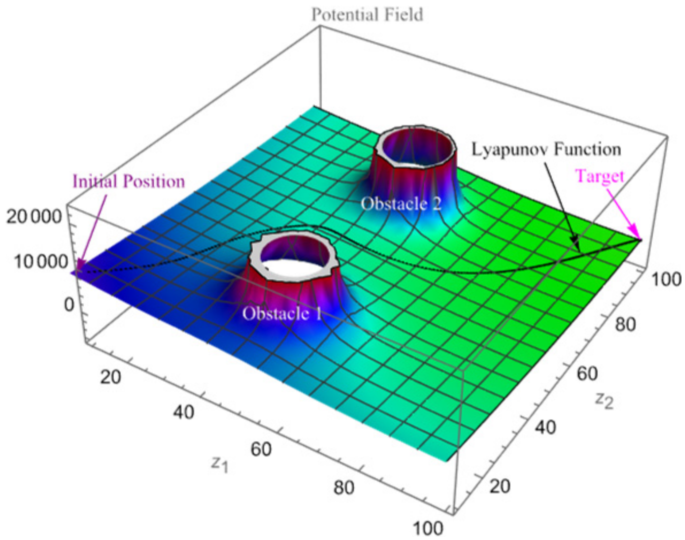

(a) 3D visualization

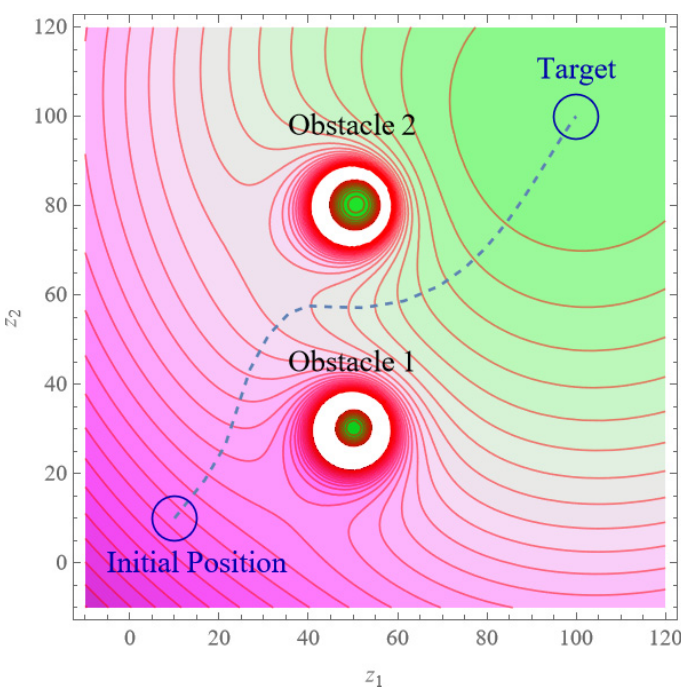

(b) Contour plot

Fig. 1. An illustration of LbCS in a workspace comprising two obstacles.

3. System Description

A new mobile manipulator, qAMM, which comprises four robotic arms fixed on rotatable bases mounted on a car-like mobile platform in a two-dimensional plane is designed in this paper. The bases can rotate through 360^o along their principal axes via revolute joints. Two articulated arms are mounted on the front of the car-like base while the other two arms are mounted on the rear, each consisting of 2 rigid links connected via revolute joints with the 2nd link having an end-effector. For each arm, given $i \in \{1,2,3,4\}$, the first link is of length l_{i1} and the second link's length is l_{i2}, while the angular positions of the revolute links at time t are $\theta_{i1}(t)$ and $\theta_{i2}(t)$ measured counterclockwise from the longitudinal axis of the car-like platform. qAMM's arms operate in the $z_1 z_2$-plane to perform assigned tasks in a two-dimensional bounded workspace. The orientation of the car-like vehicle with respect to the z_1 axis is $\theta_c(t)$, and its mobile base is centered at $\boldsymbol{\xi} = (x_c(t), y_c(t))$ which is also the reference point of the system. The distance between the front and rear axles of the car-like platform is L, and the length of each axle is L_1. The steering angle, denoted as $\theta_w(t)$, is measured with respect to the longitudinal axis of the car-like vehicle. A schematic diagram of the proposed mobile system is illustrated in Fig. 2, where the front robotic arms are denoted as Arm 1 and Arm 2, while the rear robotic arms are denoted as Arm 3 and Arm 4. To ensure a safe distance between the arms and avoid inter-arm collisions, the following assumptions are made with respect to Fig. 2.

Assumptions

(1) $l_{12} + l_{41} < L - 2\epsilon_1$,
(2) $l_{21} + l_{31} < L - 2\epsilon_1$,
(3) $l_{i2} \leq \sqrt{(\frac{L}{2} + \epsilon_1)^2 + (\epsilon_2)^2}$.

With respect to Fig. 2, the coordinate of each end-effector, suppressing t, is (x_i, y_i) for $i \in \{1,2,3,4\}$, and is given as

$$x_i = x_c + \left[(-1)^{\lceil \frac{i}{2} \rceil - \lceil \frac{i}{4} \rceil}\right] \frac{L}{2} \cos\theta_c - \left[(-1)^{\lfloor \frac{i}{2} \rfloor}\right] \frac{L_1}{2} \sin\theta_c + \sum_{j=1}^{2} l_{ij} \cos\left(\theta_c + \sum_{m=1}^{j} (\theta_{im})\right),$$

$$y_i = y_c + \left[(-1)^{\lceil \frac{i}{2} \rceil - \lceil \frac{i}{4} \rceil}\right] \frac{L}{2} \sin\theta_c + \left[(-1)^{\lfloor \frac{i}{2} \rfloor}\right] \frac{L_1}{2} \cos\theta_c + \sum_{j=1}^{2} l_{ij} \sin\left(\theta_c + \sum_{m=1}^{j} (\theta_{im})\right).$$

The coordinate (x_i, y_i), where $i \in \{1,2,3,4\}$ representing the four end-effectors, describes how the coordinates of each end-effector are influenced by the position and orientation of the robot's chassis, the lengths of revolute links, and the joint angles. They allow for the calculation of the end-effector positions based on these parameters, as follows:

- The coefficient $(-1)^{\lceil \frac{i}{2} \rceil - \lceil \frac{i}{4} \rceil}$ alternates between 1 and -1 based on the value of $\lceil \frac{i}{2} \rceil - \lceil \frac{i}{4} \rceil$. This term contributes to the x-coordinate based on the length L and the orientation of the end-effector.

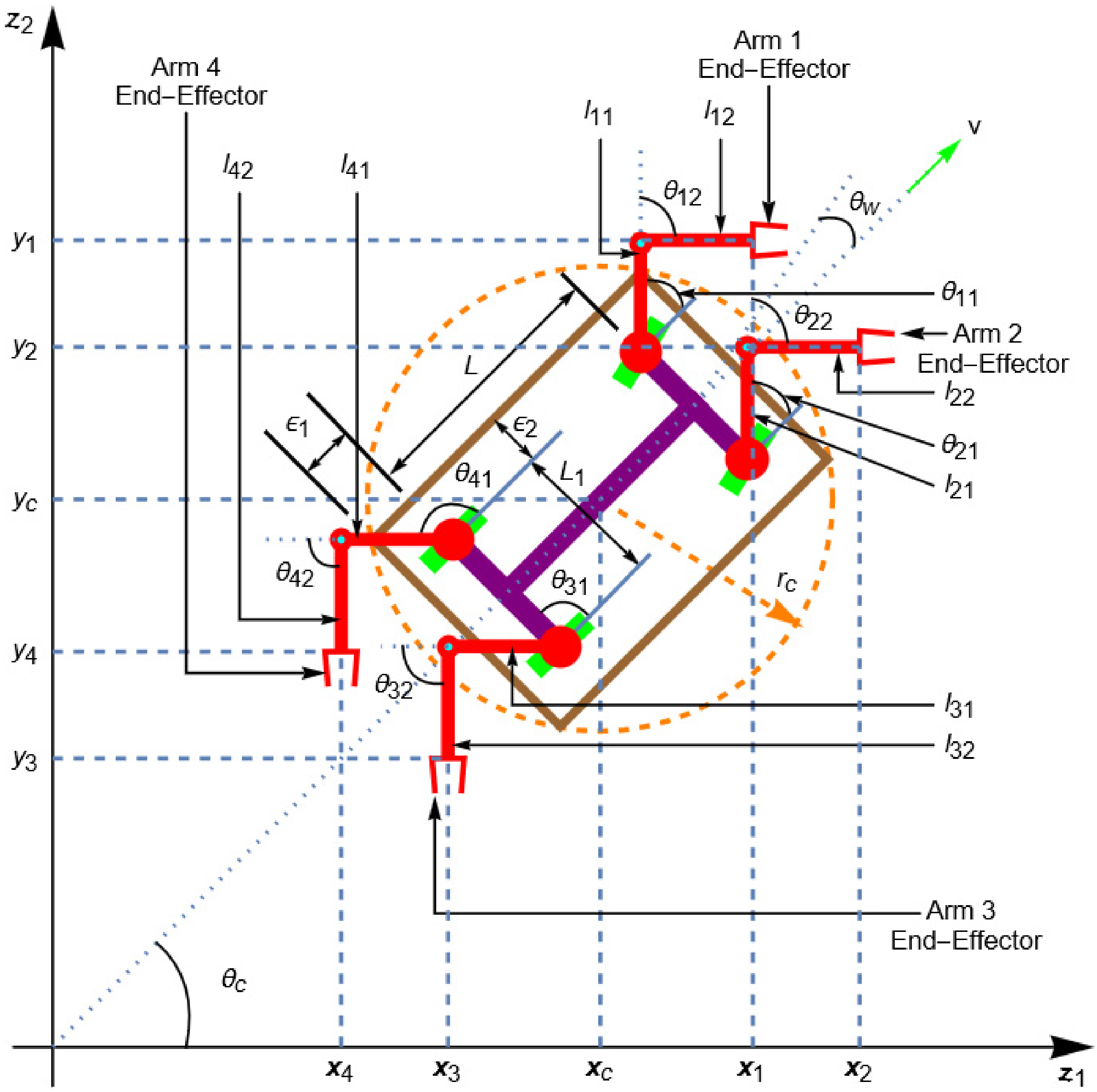

Fig. 2. Schematic representation of a four-arm car-like manipulator (qAMM) with front wheel steering and steering angle θ_w, with a dashed circle indicating the circular protective region of radius r_c.

- The coefficient $(-1)^{\lfloor \frac{i}{2} \rfloor}$ alternates between 1 and -1 based on the value of $\lfloor \frac{i}{2} \rfloor$. This term contributes to the x-coordinate based on the length L_1 and the orientation of the end-effector.
- The y_i coordinate follows a similar pattern as above, with corresponding terms involving y_c.

As shown in Fig. 2, the enclosure of qAMM in a circular protective region centered at $(x_c(t), y_c(t))$ with radius $r_c = \sqrt{(\frac{L}{2} + \epsilon_1)^2 + (\frac{L_1}{2} + \epsilon_2)^2}$, where the constants ϵ_1 and ϵ_2 are the clearance parameters, has been used from Sharma *et al.* [15] and Vanualailai *et al.* [17]. These safety parameters are added to the vehicle's dimensions L and L_1 to ensure that there is always a safe distance between qAMM and an obstacle. The nonholonomic constraints have been inherently reflected in the ordinary differential equations. For the proposed mobile manipulator, it is assumed that there is no slippage and pure rolling as the velocities which are perpendicular with respect to the wheels are zero [15]:

$$\dot{x}_{w_r} \sin\theta_c - \dot{y}_{w_r} \cos\theta_c = 0,$$
$$\dot{x}_{w_f} \sin(\theta_c + \theta_w) - \dot{y}_{w_f} \cos(\theta_c + \theta_w) = 0,$$

where $(\dot{x}_{w_r}, \dot{y}_{w_r})$ and $(\dot{x}_{w_f}, \dot{y}_{w_f})$ are the rear and front wheel velocities. Therefore, the car-like vehicle's configuration is given as $(x_c(t), y_c(t), \theta_c(t) \in \mathbb{R}^3$. The kinematic model of qAMM comprising four robotic arms, for $i \in \{1, 2, 3, 4\}$, on suppressing t, is obtained as follows:

$$\left.\begin{aligned}
\dot{x}_i &= v\cos\theta_c - \left[(-1)^{\lceil \frac{i}{2}\rceil - \lceil \frac{i}{4}\rceil}\right] Lw\sin\theta_c \\
&\quad - \left[(-1)^{\lfloor \frac{i}{2}\rfloor}\right]\frac{L_1}{2} w\cos\theta_c \\
&\quad - \left(w_c + \sum_{j=1}^{2} w_{ij}\right)\sum_{k=1}^{j-1} l_{ik}\sin\left(\theta_c + \sum_{m=1}^{k}\theta_{im}\right), \\
\dot{y}_i &= v\sin\theta_c + \left[(-1)^{\lceil \frac{i}{2}\rceil - \lceil \frac{i}{4}\rceil}\right] Lw\cos\theta_c \\
&\quad - \left[(-1)^{\lfloor \frac{i}{2}\rfloor}\right]\frac{L_1}{2} w\sin\theta_c \\
&\quad + \left(w_c + \sum_{j=1}^{2} w_{ij}\right)\sum_{k=1}^{j-1} l_{ik}\cos\left(\theta_c + \sum_{m=1}^{k}\theta_{im}\right), \\
\dot{x}_c &= v\cos\theta_c - \frac{L}{2} w\sin\theta_c, \\
\dot{y}_c &= v\sin\theta_c + \frac{L}{2} w\cos\theta_c, \\
\dot{\theta}_c &= w := \frac{v}{L}\tan\theta_w, \\
\dot{\theta}_{i1} &= w_{i1}, \dot{\theta}_{i2} = w_{i2}, \\
\dot{v} &= \mu, \dot{w} = \varpi, \\
\dot{w}_{i1} &= \sigma_{i1}, \dot{w}_{i2} = \sigma_{i2}.
\end{aligned}\right\} \tag{1}$$

The angular and translational velocities are $w(t)$ and $v(t)$, while the angular and translational accelerations are $\varpi(t)$ and $\mu(t)$, which also are the acceleration-based controllers of the car-like mobile base of qAMM.

With respect to Fig. 2, the end-effector position of the front revolute arms, Arm 1 and Arm 2, is denoted as $\boldsymbol{x_1} = (x_1(t), y_1(t))$ and $\boldsymbol{x_2} = (x_2(t), y_2(t))$, while that of the rear revolute arms, Arm 3 and Arm 4, is denoted as $\boldsymbol{x_3} = (x_3(t), y_3(t))$ and $\boldsymbol{x_4} = (x_4(t), y_4(t))$, respectively. For $i \in \{1,2,3,4\}$, the angular velocities of the robotic arms of qAMM are denoted as w_{i1} and w_{i2}, while the angular accelerations are given by σ_{i1} and σ_{i2}, which also are the acceleration-based controllers of the 2-link robotic arms.

The initial condition of qAMM where $i \in \{1,2,3,4\}$, upon suppressing t, is given as

$$\mathbf{x}_0 := \begin{bmatrix} x_{c_0} \\ 0 \\ 0 \\ \vdots \\ 0 \\ \vdots \\ 0 \\ 0 \\ 0 \end{bmatrix} + \begin{bmatrix} 0 \\ y_{c_0} \\ 0 \\ \vdots \\ 0 \\ \vdots \\ 0 \\ 0 \\ 0 \end{bmatrix} + \begin{bmatrix} 0 \\ 0 \\ \theta_{c_0} \\ \vdots \\ 0 \\ \vdots \\ 0 \\ 0 \\ 0 \end{bmatrix} + \sum_{i=1}^{4} \mathbf{x}_{i_0},$$

where

$$\mathbf{x}_{i_0} := \begin{bmatrix} 0 \\ 0 \\ 0 \\ \vdots \\ x_{i_0} \\ \vdots \\ 0 \\ 0 \\ 0 \end{bmatrix} + \begin{bmatrix} 0 \\ 0 \\ 0 \\ \vdots \\ y_{i_0} \\ \vdots \\ 0 \\ 0 \\ 0 \end{bmatrix} + \begin{bmatrix} 0 \\ 0 \\ 0 \\ 0 \\ 0 \\ \vdots \\ \theta_{i1_0} \\ \vdots \\ 0 \end{bmatrix} + \begin{bmatrix} 0 \\ 0 \\ 0 \\ 0 \\ 0 \\ 0 \\ \vdots \\ \theta_{i2_0} \\ \vdots \end{bmatrix}.$$

In addition, the state vector of qAMM for $i \in \{1,2,3,4\}$ is given as

$$\mathbf{x} := \begin{bmatrix} x_c \\ 0 \\ 0 \\ \vdots \\ 0 \\ \vdots \\ 0 \\ 0 \\ 0 \end{bmatrix} + \begin{bmatrix} 0 \\ y_c \\ 0 \\ \vdots \\ 0 \\ \vdots \\ 0 \\ 0 \\ 0 \end{bmatrix} + \begin{bmatrix} 0 \\ 0 \\ \theta_c \\ \vdots \\ 0 \\ \vdots \\ 0 \\ 0 \\ 0 \end{bmatrix} + \sum_{i=1}^{4} \mathbf{x}_i,$$

where

$$\mathbf{x}_i := \begin{bmatrix} 0 \\ 0 \\ 0 \\ \vdots \\ x_i \\ \vdots \\ 0 \\ 0 \\ 0 \end{bmatrix} + \begin{bmatrix} 0 \\ 0 \\ 0 \\ \vdots \\ y_i \\ \vdots \\ 0 \\ 0 \\ 0 \end{bmatrix} + \begin{bmatrix} 0 \\ 0 \\ 0 \\ 0 \\ 0 \\ \vdots \\ \theta_{i1} \\ \vdots \\ 0 \end{bmatrix} + \begin{bmatrix} 0 \\ 0 \\ 0 \\ 0 \\ 0 \\ 0 \\ \vdots \\ \theta_{i2} \\ \vdots \end{bmatrix}.$$

The proposed approach primarily focuses on using 2-link robotic arms due to the structure of the qAMM system, which incorporates four robotic arms mounted on a car-like platform. However, the approach could be extended to general n-link robotic arms.

The coordinate of each end-effector of qAMM comprising n-link revolute arms, suppressing t, is given as (x_i, y_i) for $i \in \{1,2,3,4\}$ and $j \in \{1,2,3,\ldots,n\}$, and is given as

$$
\begin{aligned}
x_i &= x_c + \left[(-1)^{\lceil\frac{i}{2}\rceil - \lceil\frac{i}{4}\rceil}\right]\frac{L}{2}\cos\theta_c - \left[(-1)^{\lfloor\frac{i}{2}\rfloor}\right]\frac{L_1}{2}\sin\theta_c \\
&\quad + \sum_{j=1}^{n} l_{ij}\cos\left(\theta_c + \sum_{m=1}^{j}(\theta_{im})\right), \\
y_i &= y_c + \left[(-1)^{\lceil\frac{i}{2}\rceil - \lceil\frac{i}{4}\rceil}\right]\frac{L}{2}\sin\theta_c + \left[(-1)^{\lfloor\frac{i}{2}\rfloor}\right]\frac{L_1}{2}\cos\theta_c \\
&\quad + \sum_{j=1}^{n} l_{ij}\sin\left(\theta_c + \sum_{m=1}^{j}(\theta_{im})\right).
\end{aligned}
$$

Subsequently, the kinematic model of qAMM comprising n-link robotic arms is obtained as

$$
\left.
\begin{array}{c}
\dot{x}_i = v\cos\theta_c - \left[(-1)^{\lceil\frac{i}{2}\rceil - \lceil\frac{i}{4}\rceil}\right]Lw\sin\theta_c \\
-\left[(-1)^{\lfloor\frac{i}{2}\rfloor}\right]\dfrac{L_1}{2}w\cos\theta_c \\
-\left(w_c + \displaystyle\sum_{j=1}^{n} w_{ij}\right)\displaystyle\sum_{k=1}^{j-1} l_{ik}\sin\left(\theta_c + \displaystyle\sum_{m=1}^{k}\theta_{im}\right), \\
\dot{y}_i = v\sin\theta_c + \left[(-1)^{\lceil\frac{i}{2}\rceil - \lceil\frac{i}{4}\rceil}\right]Lw\cos\theta_c \\
-\left[(-1)^{\lfloor\frac{i}{2}\rfloor}\right]\dfrac{L_1}{2}w\sin\theta_c \\
+\left(w_c + \displaystyle\sum_{j=1}^{n} w_{ij}\right)\displaystyle\sum_{k=1}^{j-1} l_{ik}\cos\left(\theta_c + \displaystyle\sum_{m=1}^{k}\theta_{im}\right), \\
\dot{x}_c = v\cos\theta_c - \dfrac{L}{2}w\sin\theta_c, \\
\dot{y}_c = v\sin\theta_c + \dfrac{L}{2}w\cos\theta_c, \\
\dot{\theta}_c = w := \dfrac{v}{L}\tan\theta_w, \\
\dot{\theta}_{i1} = w_{i1}, \dot{\theta}_{i2} = w_{i2}, \ldots, \dot{\theta}_{in} = w_{in}, \\
\dot{v} = \mu, \dot{w} = \varpi, \\
\dot{w}_{i1} = \sigma_{i1}, \dot{w}_{i2} = \sigma_{i2}, \ldots, \dot{w}_{in} = \sigma_{in}.
\end{array}
\right\}
$$

This study is a theoretical exposition into the implementation of LbCS in solving the motion planning and control problem of qAMM, focusing on the kinematic analysis of the four-arm mobile manipulator shown in Fig. 2, and the dynamic modeling of this system is open for research.

4. Targets, Obstacles and Trajectory Control of qAMM

Based on the work requirements and target location, the appropriate arms of the proposed system can perform designated tasks. Therefore, the dual-step technique utilized in [5] is adopted to navigate qAMM's car-like mobile base and its robotic arms to the pseudo-target and end-effector targets, respectively.

4.1. *The pseudo-target*

A pseudo-target is the target position of the car-like vehicle from which the four assigned targets can be accessed. An illustration of the appropriate location of the pseudo-target is shown in Fig. 3, where four garbage heaps located across a street-end are to be cleared and loaded onto a garbage truck for disposal. Such multiple tasks can be easily carried out by qAMM, whereby it has to park at a pseudo-target from where all tasks can be performed simultaneously.

Definition 4.1. The pseudo-target, which must lie in a defined neighborhood of (a_i, b_i), is taken as a disk with center $\boldsymbol{x}_{T_c} = (a_c, b_c)$ and radius ζ_{T_c}, described as

$$T_c = \{(z_1, z_2) \in \mathbb{R}^2 : (z_1 - a_c)^2 + (z_2 - b_c)^2 \le \zeta_{T_c}^2\}. \quad (2)$$

4.2. *The end-effector targets*

The ultimate end-effector targets are disk-shaped with center $\boldsymbol{x}_{T_i} = (a_i, b_i)$ and radius ς_{T_i} where $i \in \{1, 2, 3, 4\}$, and are described as the set:

$$T_i = \{(z_1, z_2) \in \mathbb{R}^2 : (z_1 - a_i)^2 + (z_2 - b_i)^2 \le \varsigma_{T_i}^2\}. \quad (3)$$

4.3. *The obstacles*

For efficient navigation while performing various tasks, the robot may encounter several fixed obstructions that can challenge its operation. These obstacles can be irregular shapes like trees, shrubs, structural elements within construction sites, factories, warehouses and fixed infrastructure such as lampposts and fire hydrants that can obstruct qAMM's path. The $k \in \mathbb{N}$ obstacles in this research are generally represented as disks, centered at $\boldsymbol{x}_{O_q} = (o_{q1}, o_{q2})$ with radius $r_{O_q} > 0$ where $q \in \{1, 2, 3, \ldots, k\}$, and described as

$$O_q = \{(z_1, z_2) \in \mathbb{R}^2 : (z_1 - o_{q1})^2 + (z_2 - o_{q2})^2 \le r_{O_q}^2\}. \quad (4)$$

4.4. *The dual-step algorithm*

Step 1: The car-like platform of qAMM moves from its initial position, (x_c, y_c) to a pseudo-target, (a_c, b_c) without any movement of the end-effectors.

Step 2: The end-effectors of qAMM will only get attracted to their ultimate targets, (a_i, b_i), when the mobile platform has moved to a region within a

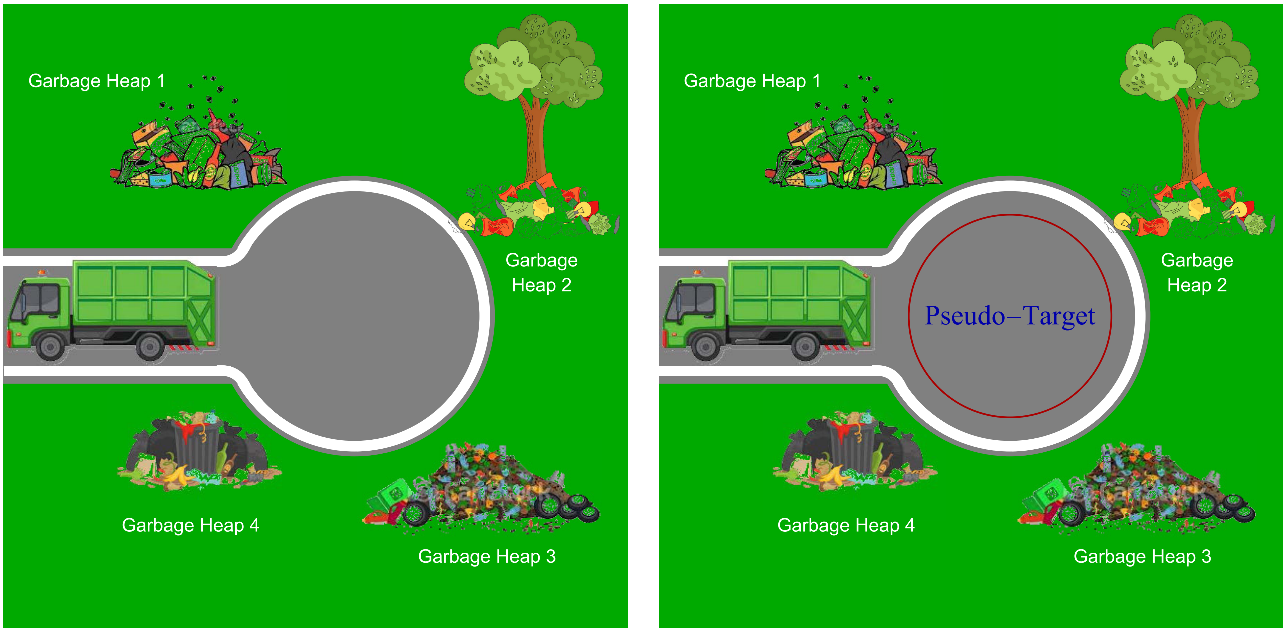

(a) Garbage heaps that are to be cleared are the end-effector targets

(b) Location of the pseudo-target from where end-effector targets can be accessed

Fig. 3. A demonstration of the appropriate location of the pseudo-target for multi-tasking operations.

user-defined distance of $r > 0$ from the pseudo-target, i.e. $(x_c - a_c)^2 + (y_c - b_c)^2 \leq r^2$.

Given $\boldsymbol{\xi} = (x_c(t), y_c(t))$, the following function, Ψ, is utilized to ensure that qAMM's end-effectors only get attracted to their targets once the car-like platform is inside the pseudo-target:

$$\Psi = \begin{cases} 0, & \|\boldsymbol{\xi} - \mathbf{x}_{T_c}\|^2 > r^2, \\ r^2 - \|\boldsymbol{\xi} - \mathbf{x}_{T_c}\|^2, & \text{otherwise.} \end{cases} \tag{5}$$

The distinct form of the function Ψ is time-dependent and plays a significant role in ensuring that qAMM's acceleration-based motion controllers are continuous. Note that $\dot{\Psi} = 0$.

4.5. *The equilibrium state*

The equilibrium state for qAMM is defined as

$$\mathbf{x}_e^* := \begin{bmatrix} a_c \\ 0 \\ 0 \\ \vdots \\ 0 \\ \vdots \\ 0 \\ 0 \\ 0 \end{bmatrix} + \begin{bmatrix} 0 \\ b_c \\ 0 \\ \vdots \\ 0 \\ \vdots \\ 0 \\ 0 \\ 0 \end{bmatrix} + \begin{bmatrix} 0 \\ 0 \\ \theta_c^* \\ \vdots \\ 0 \\ \vdots \\ 0 \\ 0 \\ 0 \end{bmatrix} + \sum_{i=1}^{4} \mathbf{x}_{e_i}^*,$$

where

$$\mathbf{x}_{e_i}^* := \begin{bmatrix} 0 \\ 0 \\ 0 \\ \vdots \\ a_i \\ \vdots \\ 0 \\ 0 \\ 0 \end{bmatrix} + \begin{bmatrix} 0 \\ 0 \\ 0 \\ \vdots \\ b_i \\ \vdots \\ 0 \\ 0 \\ 0 \end{bmatrix} + \begin{bmatrix} 0 \\ 0 \\ 0 \\ 0 \\ 0 \\ \vdots \\ \theta_{i1}^* \\ \vdots \\ 0 \end{bmatrix} + \begin{bmatrix} 0 \\ 0 \\ 0 \\ 0 \\ 0 \\ 0 \\ \vdots \\ \theta_{i2}^* \\ \vdots \end{bmatrix}$$

for $i \in \{1, 2, 3, 4\}$, and θ_c^* is the final angular orientation of the car-like mobile base.

5. Design of the Lyapunov-based Acceleration Controllers

5.1. *Lyapunov function components*

To guide qAMM along the most favorable trajectory while avoiding LbCS's local minima problem, target attraction and obstacle avoidance functions will be utilized for generating efficient paths from the robot's current position to the desired target. These functions provide a crucial mechanism for qAMM to approach desired pseudo-target and end-effector target locations, guiding the autonomous movements, navigation, and interaction with the environment.

The following obstacle avoidance function will be utilized to avoid collisions with the qth fixed obstacle where $q \in \{1, 2, 3, \ldots, k\}$:

$$H_q(\boldsymbol{x}) = \frac{1}{2}\left(\|\boldsymbol{x} - \boldsymbol{x}_{O_q}\|^2 - (r_c + r_{O_q})^2\right).$$

The arms of qAMM will not avoid the fixed obstacles while the manipulator navigates from its initial position to its pseudo-target since all four arms are enclosed inside the circular protective region. For navigation of the car-like vehicle to its pseudo-target, the attraction function is designed as

$$A(\boldsymbol{x}) = \frac{1}{2}\left(\left\|\boldsymbol{\xi} - \boldsymbol{x}_{T_c}\right\|^2 + v^2 + w^2\right). \tag{6}$$

The convergence of the articulated arm end-effectors to their assigned targets is facilitated by the attraction function given as

$$B(\boldsymbol{x}) = \frac{\Psi}{2}\left(\sum_{i=1}^{4}\|\boldsymbol{x}_i - \boldsymbol{x}_{T_i}\|^2 + \sum_{i=1}^{4}\sum_{j=1}^{2} w_{ij}^2\right). \tag{7}$$

5.2. *Mechanical restrictions and limitations*

The wheeled platform is powered by the rear wheels and will be steered by the front wheels. The car-like system must adhere to a vehicle's velocity and steering angle restrictions to avoid jackknife situations and for safety reasons. The restriction on the steering angle is given as $\theta_w(t) \le \theta_{w_{\max}} < \frac{\pi}{2}$, and is facilitated by

$$|w| < \frac{v_{\max}|\tan\theta_{w_{\max}}|}{L} := w_{\max}, \tag{8}$$

where $\theta_{w_{\max}}$ is the maximum steering angle.

In order to use LbCS, artificial obstacles must be constructed for each of the singularities and restrictions. For example, the steering angle restriction has been treated as an artificial obstacle, as shown in Fig. 4.

A function P_v guarantees that the car-like mobile base adheres to the linear velocity restrictions and is given as

$$P_v = \frac{1}{2}(v_{\max}^2 - v^2). \tag{9}$$

The function that controls the angular velocity of the car-like vehicle is proposed to be

$$P_w = \frac{1}{2}\left(\left(\frac{v_{\max}}{L}\tan\theta_{w_{\max}}\right)^2 - w^2\right). \tag{10}$$

The linear and angular velocities are restricted as $v(t) \le v_{\max}$ and $w(t) \le w_{\max}$, respectively, where $v_{\max}$ and $w_{\max}$ are the maximum linear and angular velocities of the vehicle. Setting such restrictions allows qAMM to navigate safely in its workspace.

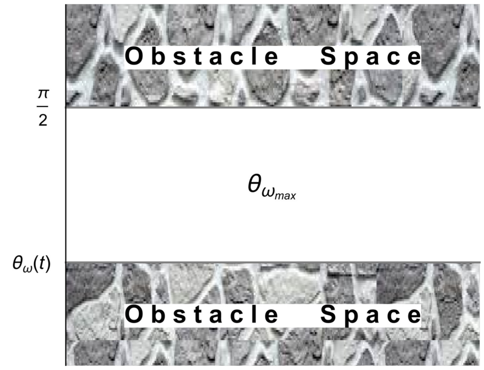

Fig. 4. The artificial obstacles that restrict the steering angle of qAMM forms the obstacle space.

To provide a precise trajectory for navigating the end-effector targets, the angular velocities of the revolute links must be controlled to prevent chaotic movements. The function that controls the angular velocities of the first and second links of the revolute arms of qAMM is described as

$$Q_i = \frac{1}{2}\left(\sum_{i=1}^{4}\left(w_{i1_{\max}}^2 - w_{i1}^2\right) + \sum_{i=1}^{4}\left(w_{i2_{\max}}^2 - w_{i2}^2\right)\right), \tag{11}$$

where $w_{i1}(t) \le w_{i1_{\max}}$ and $w_{i2}(t) \le w_{i2_{\max}}$ for $i \in \{1, 2, 3, 4\}$. The second links of all articulated arms cannot fully fold onto their corresponding first links while performing either clockwise or counterclockwise rotation. The singularities of the 2nd links of all the arms arise when $\theta_{i2} = |\theta_{i2_{\max}}|$, and the function given below is utilized to account for these singularities:

$$S_i = \theta_{i2_{\max}} - |\theta_{i2}|,$$

where $i \in \{1, 2, 3, 4\}$.

5.3. *Lyapunov function*

LbCS, which operates within the artificial potential framework, is employed to design the continuous time-invariant motion control laws. The attractive and repulsive potential field functions used in Eq. (12) are developed using the distance functions. The attractive potential function at an arbitrary time is the measure of the Euclidean distance between the target and a robot, usually multiplied by the target convergence parameter. The target convergence parameter represents the strength of attraction between the target and the robot. A larger parameter value indicates that the robot converges faster to its target. On the other hand, the repulsive potential function for stationary obstacle avoidance at an arbitrary time is a measure of the ratio of an obstacle avoidance parameter to the Euclidean distance between the stationary obstacle and the robot. The obstacle avoidance parameter represents the repulsion strength between the stationary obstacle and the robot. A larger avoidance parameter value indicates that the robot will experience greater repulsion as it approaches the obstacle. Subsequently, these functions are part of a total potential function called the Lyapunov function from which the time-invariant nonlinear acceleration controllers are extracted.

Let $\rho_i > 0$, $\kappa > 0$, $\lambda > 0$, $\gamma_q > 0$ and $\beta_i > 0$ be the control parameters. A Lyapunov function, for $i \in \{1, 2, 3, 4\}$ and $q \in \{1, 2, 3, \ldots, k\}$, is defined as

$$\pounds(\mathbf{x}) = A(\mathbf{x}) + B(\mathbf{x}) + D(\mathbf{x})\left(\frac{\kappa}{P_v} + \frac{\lambda}{P_w}\right) + D(\mathbf{x})\left(\sum_{q=1}^{k}\frac{\gamma_q}{H_q} + \sum_{i=1}^{4}\frac{\rho_i}{Q_i} + \sum_{i=1}^{4}\frac{\beta_i}{S_i}\right). \tag{12}$$

To ensure that the Lyapunov function vanishes after qAMM has converged to its final orientation, a function whose role is purely mathematical, and hence, auxiliary, is utilized in Eq. (12). This auxiliary function guarantees that the nonlinear acceleration-based controllers will vanish at the ultimate target, and is introduced as

$$D(\mathbf{x}) = \frac{1}{2}(\|\boldsymbol{\xi} - \mathbf{x}_{T_c}\|^2) + \frac{\Psi}{2}\left(\sum_{i=1}^{4}\|\mathbf{x}_i - \mathbf{x}_{T_i}\|^2\right). \tag{13}$$

5.4. *Controller design*

Careful design of the motion controllers is vital to help achieve the proposed car-like system's stability, help facilitate the movement of different system components and execute designated tasks. In addition to the movement of the proposed car-like vehicle, the controllers are also responsible for facilitating the smooth motion of all the robotic arms and the four end-effectors within the system's workspace. The design of qAMM's controllers is appropriately shown by the control scheme in the block diagram provided in Fig. 5.

Along a trajectory obtained from system (1),

$$\begin{aligned}\dot{\pounds}(\mathbf{x}) &= \dot{A}(\mathbf{x}) + \dot{B}(\mathbf{x}) + \dot{D}(\mathbf{x})\left(\frac{\kappa}{P_v} + \frac{\lambda}{P_w}\right)\\ &\quad + \dot{D}(\mathbf{x})\left(\sum_{q=1}^{k}\frac{\gamma_q}{H_q} + \sum_{i=1}^{4}\frac{\rho_i}{Q_i} + \sum_{i=1}^{4}\frac{\beta_i}{S_i}\right)\\ &\quad - D(\mathbf{x})\left(\frac{\kappa\dot{P}_v}{{P_v}^2} + \frac{\lambda\dot{P}_w}{{P_w}^2} + \sum_{q=1}^{k}\frac{\gamma_i\dot{H}_q}{H_q^2}\right)\\ &\quad - D(\mathbf{x})\left(\sum_{i=1}^{4}\frac{\rho_i\dot{Q}_i}{Q_i^2} + \sum_{i=1}^{4}\frac{\beta_i\dot{S}_i}{S_i^2}\right),\end{aligned} \tag{14}$$

which, after collecting terms comprising v, w, and w_{ij}, is rearranged as

$$\dot{\pounds}(\mathbf{x}) = f_1 v + f_2 w + \sum_{i=1}^{4}\sum_{j=1}^{2} f_{ij} w_{ij},$$

where the functions f_1, f_2, and f_{ij} for $i \in \{1, 2, 3, 4\}$ and $j \in \{1, 2\}$, upon suppressing $\mathbf{x}$, are

$$\begin{aligned} f_1 &= \mu + \frac{\kappa D}{{P_v}^2}\mu + \frac{\partial\pounds}{\partial x_c}\cos\theta_c + \frac{\partial\pounds}{\partial y_c}\sin\theta_c,\\ f_2 &= \varpi + \frac{\lambda D}{{P_w}^2}\varpi + \frac{\partial\pounds}{\partial\theta_c} - \frac{\partial\pounds}{\partial x_c}\frac{L}{2}\sin\theta_c + \frac{\partial\pounds}{\partial y_c}\frac{L}{2}\cos\theta_c,\\ f_{ij} &= \sigma_{ij} + \frac{\partial\pounds}{\partial\theta_{ij}} + \frac{\rho_i D}{Q_i^2}\sigma_{ij}.\end{aligned}$$

5.5. *Control laws*

Thus, the acceleration-based motion controllers, μ, ϖ and σ_{ij}, of qAMM are obtained as

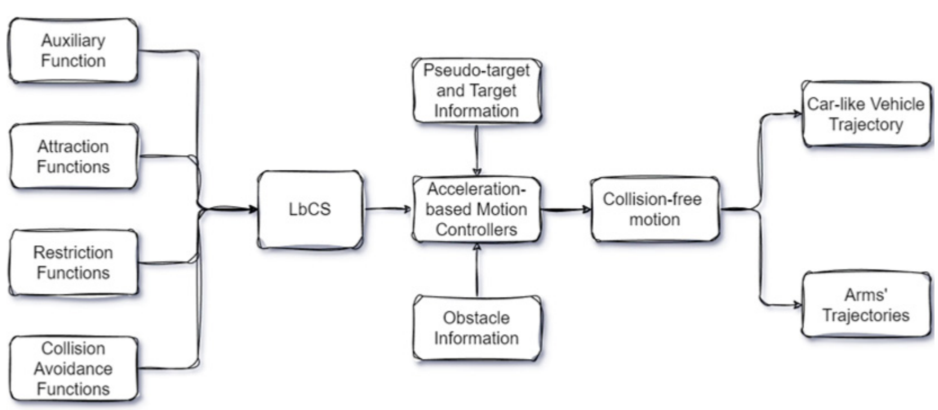

Fig. 5. An illustration of qAMM's control scheme.

$$\left.\begin{aligned}\mu &= -\frac{1}{1+\frac{\kappa D}{P_v^2}}\left(\eta_1 v + \cos\theta_c \frac{\partial \mathcal{L}}{\partial x_c} + \sin\theta_c \frac{\partial \mathcal{L}}{\partial y_c}\right),\\ \varpi &= \frac{1}{1+\frac{\lambda D}{P_w^2}}\left(-\eta_2 w + \frac{L}{2}\sin\theta_c \frac{\partial \mathcal{L}}{\partial x_c} - \frac{L}{2}\cos\theta_c \frac{\partial \mathcal{L}}{\partial y_c} - \frac{\partial \mathcal{L}}{\partial \theta_c}\right),\\ \sigma_{ij} &= -\frac{1}{1+\sum_{i=1}^{4}\frac{\rho_i D}{Q_i^2}}\left(\sum_{i=1}^{4}\sum_{j=1}^{2}\eta_{i+2} w_{ij} + \sum_{i=1}^{4}\sum_{j=1}^{2}\frac{\partial \mathcal{L}}{\partial \theta_{ij}}\right)\end{aligned}\right\}, \tag{15}$$

where

- μ is the linear acceleration controller of the car-like vehicle,
- ϖ is the angular acceleration controller of the car-like vehicle,
- σ_{ij} is the angular acceleration controller of the 2-link robotic arms,
- $\eta_1 > 0$, $\eta_2 > 0$, and $\eta_{i+2} > 0$ are the convergence parameters.

6. Stability Analysis of the System

Stability analysis of robotics systems plays an essential role in studying motion control techniques. The control laws designed in Eq. (15) have been formulated from the Lyapunov function given in Eq. (12), $\mathcal{L}(\mathbf{x})$. A mathematical proof provided below shows the stability of system (1).

Let $\eta_1 > 0$, $\eta_2 > 0$, and $\eta_{i+2} > 0$ be the convergence parameters for $i \in \{1,2,3,4\}$. Then, with respect to system (1),

$$\dot{\mathcal{L}}(\mathbf{x}) = -\left(\eta_1 v^2 + \eta_2 w^2 + \sum_{i=1}^{4}\sum_{j=1}^{2}\eta_{i+2} w_{ij}^2\right) \le 0,$$
$$\forall \mathbf{x} \in D(\mathcal{L}(\mathbf{x})).$$

The direct method of Lyapunov aims at determining the stability properties of $\mathbf{x}_e^*$ and its relationship with a positive definite Lyapunov function $\mathcal{L}(\mathbf{x})$. The equilibrium point of system (1) is $\mathbf{x}_e^*$, and $\mathcal{L}(\mathbf{x})$ is a Lyapunov function on $D(\mathcal{L}(\mathbf{x}))$ that guarantees the stability of the proposed car-like system. The stability analysis of qAMM is summarized appropriately in Theorem (6.1):

Theorem 6.1. *The equilibrium point $\mathbf{x}_e^*$, as given in* (4.5)*, is a stable point given the acceleration-based controllers of qAMM are defined as in (15).*

Proof. (1) $\mathcal{L}(\mathbf{x})$ is positive and defined on the domain given as

$$\begin{aligned} D(\mathcal{L}(\mathbf{x})) = \{\mathbf{x} \in \mathbb{R}^{n+13} : {}& P_v > 0, P_w > 0,\\ & Q_i \ge 0\ \forall i = \{1,2,3,4\},\\ & S_i > 0\ \forall i = \{1,2,3,4\}\}.\end{aligned}$$

(2) $\mathcal{L}(\mathbf{x})$ is continuous function and its first partial derivatives are in $D(\mathcal{L}(\mathbf{x}))$ which is in the neighborhood of the point $\mathbf{x}_e^*$ of system (1).
(3) $\mathcal{L}(\mathbf{x}_e^*) = 0$, $\mathbf{x}_e^* \in D(\mathcal{L}(\mathbf{x}))$.
(4) $\dot{\mathcal{L}}(\mathbf{x}) \le 0$, $\forall \mathbf{x} \in D(\mathcal{L}(\mathbf{x}))$.
(5) $\dot{\mathcal{L}}(\mathbf{x}_e^*) = 0$, $\mathbf{x}_e^* \in D(\mathcal{L}(\mathbf{x}))$. □

7. Convergence Analysis of the System

This section provides a theoretical exposition of the convergence of the proposed Lyapunov-based control laws using the convergence criterion of LaSalle's invariance principle, which is widely utilized in control theory to investigate the stability properties of solutions of nonlinear systems of differential equations in $\mathbb{R}^n$ and assess convergence to proper and established invariant sets.

Definition 7.1 ([23]). A set $D(\mathcal{L}(\mathbf{x}))$ is called an invariant set of system (1) if any solution $\mathbf{x}(t)$ which starts from a point in $D(\mathcal{L}(\mathbf{x}))$ at some time t_a also remains in $D(\mathcal{L}(\mathbf{x}))$ at all times:

$$\mathbf{x}(t_a) \in D(\mathcal{L}(\mathbf{x})) \Rightarrow \mathbf{x}(t) \in D(\mathcal{L}(\mathbf{x})), \forall t \in \mathbb{R}.$$

This implies that the set of all equilibrium points is an invariant set. In addition, the domain of attraction of an equilibrium point is also an invariant set. According to LaSalle [24], bounded solutions converge to the largest invariant subset of the set where the derivative of a suitable energy function is zero. In this research, LaSalle's invariance principle is utilized to prove that the individual solutions approach the desired final configuration in space or remain near the equilibrium state when time goes to infinity, as defined below.

Definition 7.2 ([24]). Let ε and T be positive real numbers and $\mathbf{x}(t)$ be a function of time. Let $\mathbf{x}_e^*$ be the set of all points $p \in D(\mathcal{L}(\mathbf{x}))$ such that $\dot{\mathcal{L}}(p) = 0$. Then, $\mathbf{x}(t)$ approaches a set $\mathbf{x}_e^*$ as t approaches infinity, denoted by $\mathbf{x}(t) \to \mathbf{x}_e^*$ as $t \to \infty$, if

$$\forall \varepsilon > 0, \exists T > 0, \forall t > T, \exists p \in \mathbf{x}_e^*, \|\mathbf{x}(t) - p\| < \varepsilon.$$

As appropriately stated in Theorem (6.1) and illustrated in Fig. 6(c), the Lyapunov function $\mathcal{L}(\mathbf{x})$ gradually vanishes as

$$\lim_{t\to+\infty} \mathcal{L}(\mathbf{x}) = 0,$$

which is the lower bound of $\mathcal{L}(\mathbf{x})$.

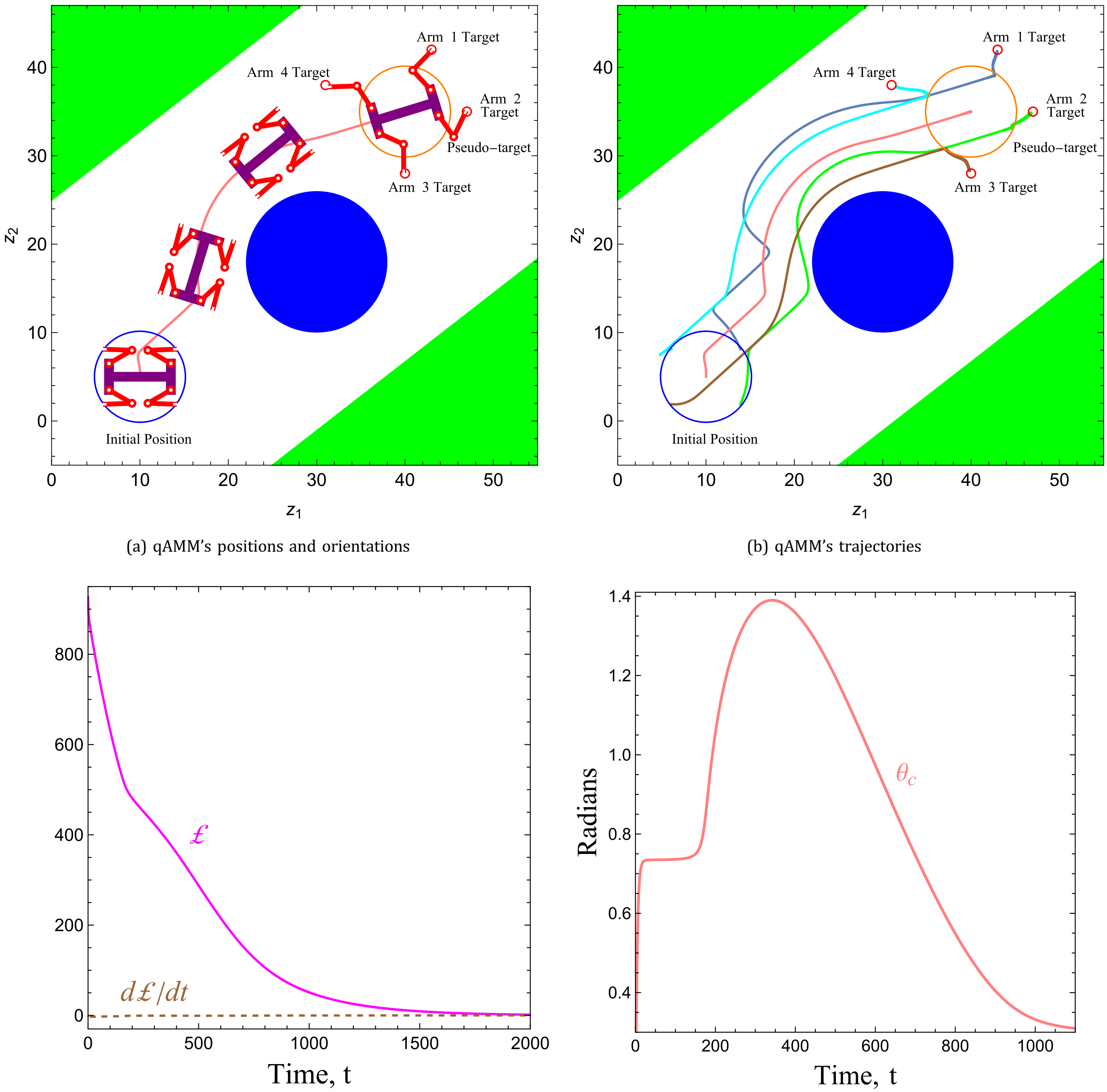

(a) qAMM's positions and orientations

(b) qAMM's trajectories

(c) Lyapunov function

(d) Angle vs time graph

Fig. 6. (a) qAMM's positions at times $t = 1, 250, 730$ and 20000 along its trajectory. (b) The car-like vehicle's trajectory is traced in pink, while that of arms 1, 2, 3 and 4 are traced in thistle, green, brown, and cyan, respectively. (c) Monotonically decreasing Lyapunov function with its time derivative. (d) Orientations of car-like vehicle. (e) The fluctuations in the linear velocity graph show that after avoiding collision with the fixed obstacle, qAMM gained speed and then slowed down on approach to its target. Its maximum velocity was set at 2. (f) The fluctuations in the angular velocity graph demonstrate that qAMM's car-like mobile base performed rotational motion as it moved from its initial position and maintained a straight path until it approached the obstacle, where it adjusted its direction and made a slight turn to avoid it before gradually stabilizing its motion to reach the target.

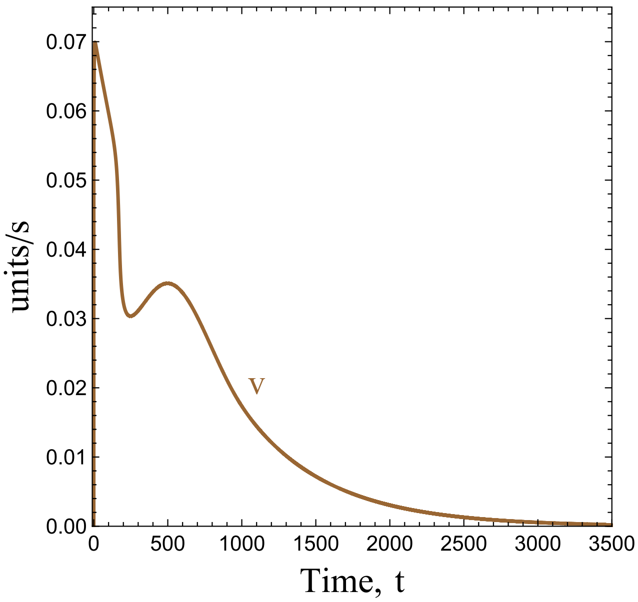

(e) Linear velocity graph

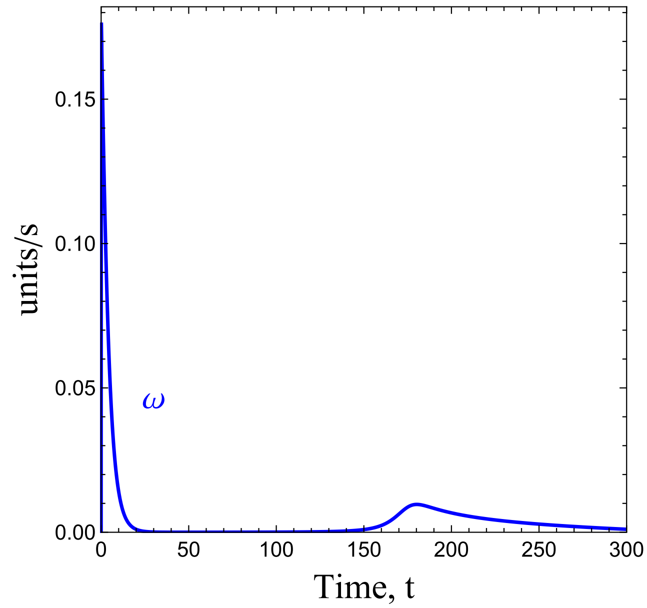

(f) Angular velocity graph

Fig. 6. (*Continued*)

Theorem 7.3. *Suppose there is a scalar function $\mathcal{L}(\mathbf{x})$ defined as in (12) which has continuous first order partial derivatives in $D(\mathcal{L}(\mathbf{x}))$ and is such that $\dot{\mathcal{L}}(p) \leq 0$ in $D(\mathcal{L}(\mathbf{x}))$. Let $\mathbf{x}_e^*$ be the set of points $p \in D(\mathcal{L}(\mathbf{x}))$ such that $\dot{\mathcal{L}}(p) = 0$. Let $N \in D(\mathcal{L}(\mathbf{x}))$ and $\mathbf{x}_e^*$ be the largest invariant set in N. Then, $\exists$ a solution $\mathbf{x}$ starting in $D(\mathcal{L}(\mathbf{x}))$ such that $\mathbf{x}(t) \to \mathbf{x}_e^*$ as $t \to \infty$.*

Proof. Let $\mathbf{x}(t)$ be a function of time. By continuity of the Lyapunov function given in Eq. (12), the function $\mathcal{L}(\mathbf{x}(t))$ is bounded. Since $\dot{\mathcal{L}}(\mathbf{x}) \leq 0, \forall \mathbf{x} \in D(\mathcal{L}(\mathbf{x}))$, the function $\mathcal{L}(\mathbf{x}(t))$ is non-increasing. Therefore, the limit of $\mathcal{L}(\mathbf{x}(t))$ must exist and is finite, and is denoted as $\daleth$:

$$\lim_{t\to\infty} \mathcal{L}(\mathbf{x}(t)) = \daleth.$$

Let an arbitrary point be $z \in \mathbf{x}_e^*$ in the ω-limit set $\mathbf{x}_e^* \subseteq N$, which is a set of points that $\mathcal{L}(z)$ approaches as time approaches infinity. Then, by the definition of ω-limit sets, there is a sequence k_t in $\mathbb{R}$ such that

$$\mathbf{x}(k_t) \to z, t \to \infty.$$

By the continuity of $\mathcal{L}(\mathbf{x}(t))$, it follows that

$$\mathcal{L}(z) = \lim_{t\to\infty} \mathcal{L}(\mathbf{x}(k_t)) = \lim_{t\to\infty} \mathcal{L}(\mathbf{x}(t)) = \daleth.$$

This implies that for all z in the ω-limit set $\mathbf{x}_e^*$, the function $\mathcal{L}(\mathbf{x}(t))$ has the same value:

$$\mathcal{L}(\mathbf{x}(t)) = \daleth, \forall z \in \mathbf{x}_e^*.$$

By the invariance of $\mathbf{x}_e^*$, if $z \in \mathbf{x}_e^*$, then $\mathbf{x}(t) \in \mathbf{x}_e^*\ \forall t \in \mathbb{R}$ which implies that $\mathcal{L}(\mathbf{x}(t)) = \daleth \forall t \in \mathbb{R}$, that is, a constant function of time, t, and must have a derivative of zero, as shown in Theorem (6.1). Therefore, $\mathbf{x}_e^*$ is an invariant set, and $\mathbf{x}(t)$ converges to $\mathbf{x}_e^*$ as $t \to \infty$. □

According to Theorem (6.1), the equilibrium point $\mathbf{x}_e^*$ is stable and all individual solutions of (15) converge to their final configurations $\mathbf{x}_e^*$, where $\mathcal{L}(\mathbf{x}_e^*) \equiv 0$, given $\mathbf{x}_e^* \in D(\mathcal{L}(\mathbf{x}))$, as $\dot{\mathcal{L}}(\mathbf{x})$ is negative definite. While Theorem (6.1) establishes that the equilibrium point $\mathbf{x}_e^*$, of system (1) is stable where $\mathcal{L}(\mathbf{x}_e^*) \equiv 0$, Theorem (7.3) sharpens this result by establishing the convergence of the bounded solutions of system (1) to the invariant set $\mathbf{x}_e^*$, which is a subset of N.

8. Results and Simulations

This section demonstrates the multi-tasking capabilities of qAMM in an obstacle-ridden environment and numerically verifies the stability results obtained from (12). The effectiveness of the proposed method was numerically verified using the Runge–Kutta Method, while the results and computer simulations were produced using the Wolfram Mathematica 11.2 software. A series of Mathematica commands were carried out to attain the simulation results. The brute-force technique was utilized to determine the restrictions, limitations and convergence parameter values tagged to the proposed quad-arm car-like mobile manipulator. Based on the target location, an invariant set of initial conditions can only facilitate a smooth trajectory of qAMM as it converges to its pseudo-target and targets. The dynamic constraints, limitations and acceleration controllers allow qAMM to trace the desired path. The initial configurations of the proposed system have to be defined in the sequence of commands to be executed. Table 1 shows the parameters that need to be defined for $i \in \{1, 2, 3, 4\}$, $j \in \{1, 2\}$ and $q \in \{1, 2, 3, \ldots, k\}$.

8.1. *Scenario 1*

Real-life tasks that must be performed collaboratively, such as garbage collection, construction, maintenance, and cleaning, are essentially the end-effector targets. In this scenario, qAMM, initially positioned at (10,5), is assigned four targets that its end-effectors must perform asynchronously. The targets are denoted as Target 1, Target 2, Target 3 and Target 4. qAMM has to avoid an obstacle and perform the four different tasks from its pseudo-target using the asynchronized motion of its revolute arms. Table 2 provides the numerical values of initial configurations, control, avoidance and convergence variables used in this scenario. The coordinates of the obstacle, pseudo-target and end-effector targets are shown in Fig. 6(a), which also indicates qAMM's navigation along its path from its initial position to its final configuration. While navigating from the initial position to the pseudo-target, only the car-like mobile base moves without any movement from the four revolute arms. The end-effectors only get attracted to their assigned targets once the vehicular base has reached the pseudo-target, thus demonstrating qAMM's effectiveness in applying the dual-step algorithm for its motion. Figure 6(b) illustrates the trajectories of the car-like base and the four end-effectors. Figure 6(c) shows the profile of the Lyapunov function, $\mathcal{L}$, with its time derivative along the system's trajectory. The evolution of the car-like vehicle's angular orientation with respect to the z_1 axis is shown in Fig. 6(d). As qAMM approaches its pseudo-target, its linear velocity and angular velocity gradually decrease to zero as shown in Figs. 6(e)

Table 1. Parameter table.

Dimensions	
Car-like vehicle	$L \times L_1$
Safety parameters	ϵ_1, ϵ_2
Length of revolute links	l_{ij}
Initial configurations	
qAMM's position	(x_{c_0}, y_{c_0})
qAMM's orientation	θ_{c_0}
Revolute links' angular orientations	θ_{ij_0}
Maximum values	
Linear velocity of car-like vehicle	$v_{\max}$
Angular velocity of car-like vehicle	$\omega_{\max}$
Angular orientation of the 2nd links of each arm	$\theta_{i2_{\max}}$
Angular velocity of revolute links	$\omega_{ij_{\max}}$
Restriction parameters	
Linear velocity	κ
Angular velocity	λ
Revolute link angular orientation	β_i
Revolute link angular velocity	ρ_i
Control parameters	
Car-like vehicle's linear velocity convergence	η_1
Car-like vehicle's angular velocity convergence	η_2
Revolute link angular velocity convergence	η_{i+2}
Obstacle avoidance	γ_q
Obstacles and targets	
Number of obstacles	k
Pseudo-target	(a_c, b_c)
End-effector targets	(a_i, b_i)

Table 2. Numerical values of parameters used in Scenario 1.

Dimensions	
$L \times L_1$	7×3
$\epsilon_1 = \epsilon_2$	1
l_{ij}	3
Initial configurations	
(x_{c_0}, y_{c_0})	(10,5)
θ_{c_0}	0
θ_{ij_0}	$\theta_{11_0} = \frac{5\pi}{6}, \theta_{12_0} = \theta_{32_0} = \frac{-37\pi}{45}$, $\theta_{21_0} = \frac{-5\pi}{6}, \theta_{22_0} = \theta_{42_0} = \frac{37\pi}{45}$, $\theta_{31_0} = \frac{-\pi}{6}, \theta_{41_0} = \frac{\pi}{6}$
Maximum values	
$v_{\max} = \omega_{\max}$	2
$\theta_{i2_{\max}}$	$\frac{5\pi}{6}$
$\omega_{ij_{\max}}$	5
Restriction parameters	
κ	0.01
λ	0.002
β_i	0.000003
ρ_i	0.0002
Control parameters	
$\eta_1 = \eta_2$	600
η_{i+2}	10
γ_q	0.1
Obstacles and targets	
k	1
(a_c, b_c)	(40,35)
(a_i, b_i)	$(a_1, b_1) = (43, 42)$, $(a_2, b_2) = (47, 35)$, $(a_3, b_3) = (40, 28)$, $(a_4, b_4) = (31, 38)$

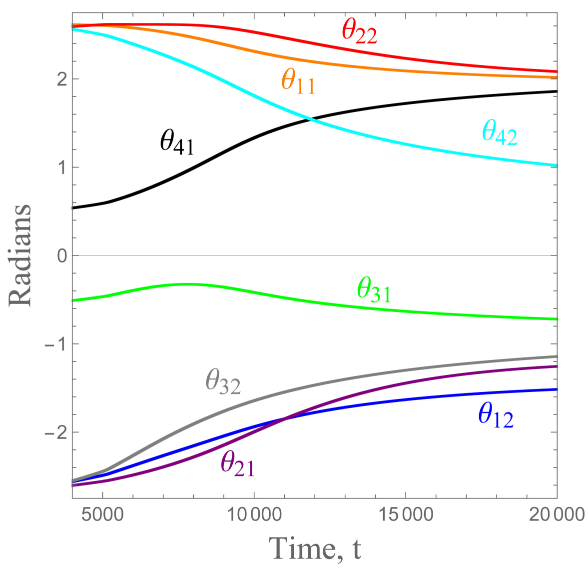

(a) Revolute link orientations

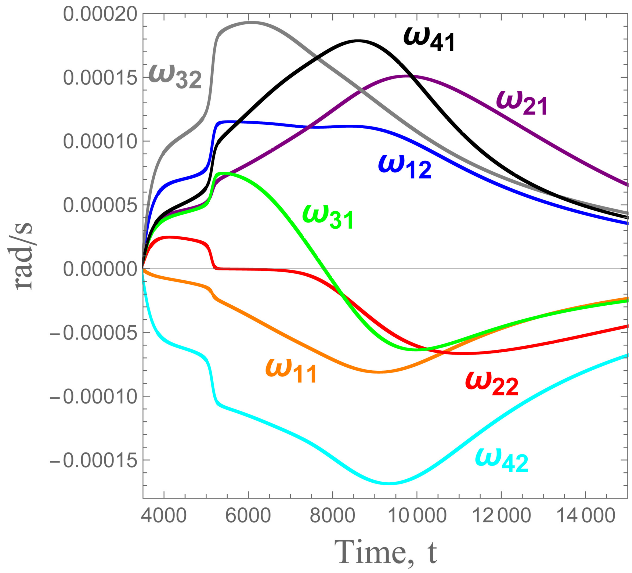

(b) Revolute link angular velocities

Fig. 7. (a) Orientations of qAMM's revolute links abiding the angular restrictions and limitations. (b) Angular velocities of qAMM's revolute links.

and 6(f), respectively. After the car-like vehicle has reached its pseudo-target positioned within the vicinity of the ultimate end-effector targets, the four revolute arms of qAMM navigate through the workspace, allowing the end-effectors to reach their ultimate targets. The evolution of the orientation angles of all eight revolute links of qAMM, which are of equal length, is shown in Fig. 7(a). Finally, the angular velocities of all the revolute links along the trajectory are illustrated in Fig. 7(b), which tend to zero as the four end-effectors approach their designated targets.

8.2. *Scenario 2*

This scenario illustrates the effectiveness of the proposed control laws in enabling qAMM to perform assigned tasks synchronously. The two left arms of qAMM, arms 1 and 4, are allocated Target A, while the two right arms, arms 2 and 3, are designated Target B, respectively. The respective arms must operate synchronously to perform the two assigned tasks. Out of the eight randomly generated obstacles of various sizes in this scenario, qAMM has to avoid those that fall in its way and maneuver to its ultimate targets located on either side of the pseudo-target. As depicted by Fig. 8(a), all the links of the revolute arms are of equal length; however, the link sizes are slightly longer in this scenario compared to Scenario 1. Table 3 provides the initial constraints, conditions, and parameters utilized if different from Scenario 1. The initial position, motion, and each of the four revolute arms orientations is shown in Fig. 8(a). The trajectory of qAMM as it navigates towards the pseudo-target and targets A and B is illustrated in Fig. 8 (b). The behavior of the orientation angles and the evolution of the angular velocities of all revolute links abiding by the limitations and restrictions tagged to qAMM's robotic arms are demonstrated in Figs. 8(c) and 8(d), respectively. The profile of the Lyapunov function and the car-like mobile base's angular orientation and linear and angular velocities are similar to that of Scenario 1. In Fig. 9, snapshots have been taken which explicitly show the end-effectors converging to their targets simultaneously in synchronous motion.

8.3. *Scenario 3*

This scenario considers the proposed system being subjected to perform tasks both synchronously and asynchronously in an environment comprising eight randomly generated obstacles of different sizes. The two front arms are delegated the same task, which they must perform synchronously. In comparison, the two rear arms are allocated entirely different tasks, which they must do asynchronously, implying that qAMM has to converge to three targets. As depicted by Fig. 10(a), all of qAMM's arms have equal-sized revolute links. First, the car-like vehicle has to navigate to its pseudo-target; after that, the four revolute arms extend their links to reach the three end-effector targets. Only those parameters different from the ones given in Scenario 1 are provided in Table 4. The initial position, motion, and orientations of revolute arms are illustrated in Fig. 10(a), while the trajectory of qAMM as it

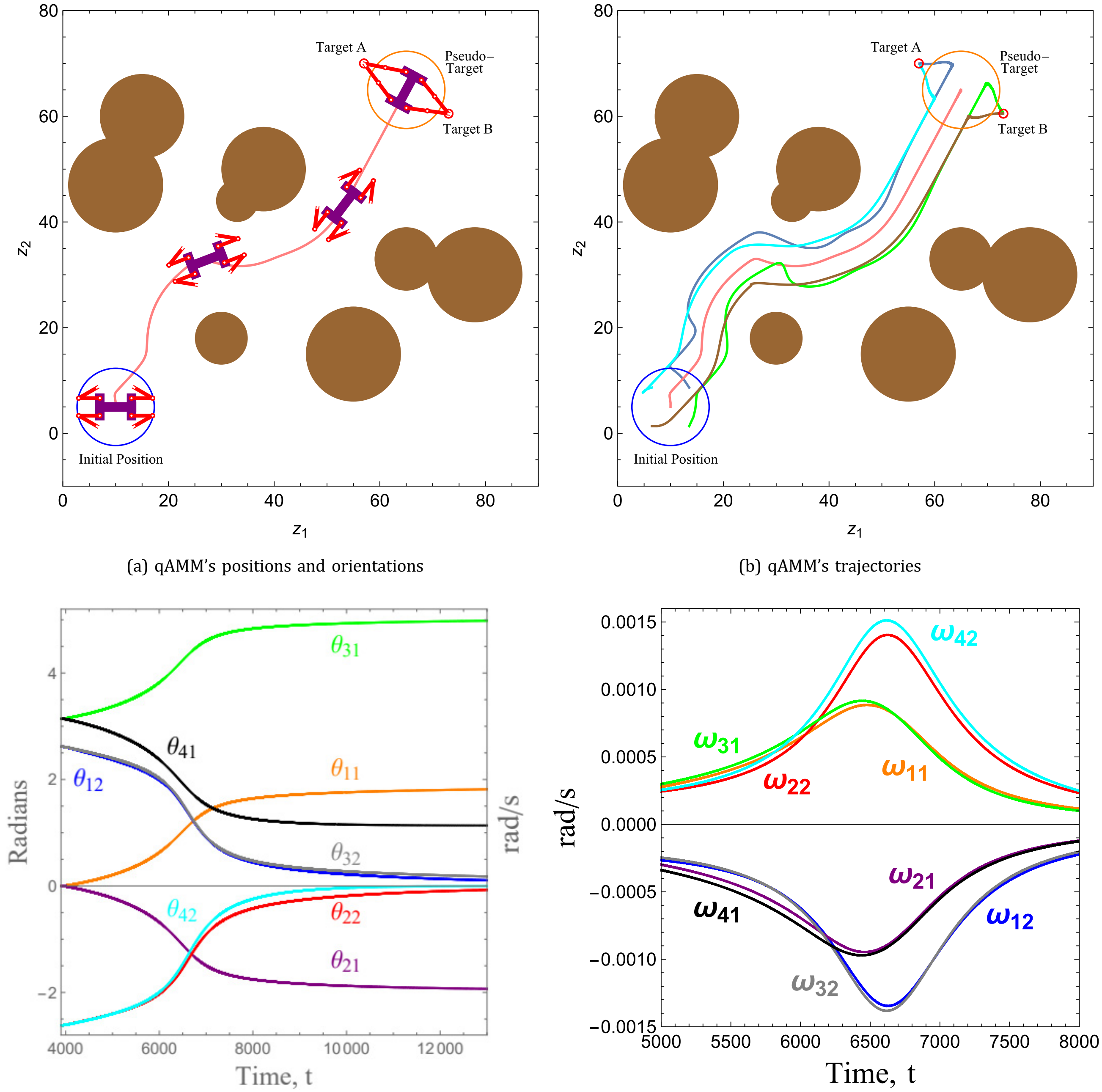

(a) qAMM's positions and orientations

(b) qAMM's trajectories

(c) Revolute link orientations

(d) Revolute link angular velocities

Fig. 8. (a) qAMM's positions at times $t = 1, 350, 900$ and 60000. (b) The car-like vehicle's trajectory is traced in pink, while that of arms 1, 2, 3 and 4 are traced in thistle, green, brown, and cyan, respectively. (c) Orientations of qAMM's revolute links. (d) Angular velocities of qAMM's revolute links.

maneuvers to its targets are shown in Fig. 10(b). The angular orientations and velocities of the revolute links abiding system limitations and restrictions are illustrated in Figs. 10(c) and 10(d). The profile of the Lyapunov function and the car-like mobile base's angular orientation and linear and angular velocities are similar to that of Scenario 1.

Remark The results indicate that the autonomous quad-arm mobile manipulator system successfully implemented the dual-step algorithm and the acceleration-based controllers to accomplish multiple assigned tasks in obstacle-ridden environments. The acceleration-based motion controllers enabled qAMM's revolute links to undergo synchronized and asynchronized motion as required. While

Table 3. Numerical values of parameters used in Scenario 2.

Dimensions	
$L \times L_1$	6×3.3
$\epsilon_1 = \epsilon_2$	2.8
l_{ij}	4
Initial configurations	
(x_{c_0}, y_{c_0})	(10,10)
θ_{ij_0}	$\theta_{11_0} = \theta_{21_0} = 0, \theta_{12_0} = \theta_{32_0} = \frac{5\pi}{6}$, $\theta_{22_0} = \theta_{42_0} = \frac{-5\pi}{6}, \theta_{31_0} = \theta_{41_0} = \pi$
Maximum values	
$\theta_{i2_{\max}}$	$\frac{8\pi}{9}$
Restriction parameters	
ρ_i	5×10^{-9}
Control parameters	
η_{i+2}	0.5
γ_q	0.6
Obstacles and targets	
k	8
(a_c, b_c)	(65,65)
(a_i, b_i)	Target A $= (a_1, b_1) = (a_4, b_4) = (57, 70)$, Target B $= (a_2, b_2) = (a_3, b_3) = (73, 60.5)$

addressing noise disturbance was not part of the scope of this study, it is evident in the literature that LbCS controllers are robust in terms of noise disturbances. For a detailed account of the robustness of LbCS controllers, the reader is referred to [25]. In situations where obstacles are introduced in the vicinity of the pseudo-target, qAMM is designed to navigate around them to reach the pseudo-target successfully. However, while qAMM can effectively bypass these obstacles, not all end-effectors will be able to access their ultimate targets due to the positioning of the obstacles obstructing the end-effectors' paths. The collision-avoidance scheme of qAMM ensures its safety in such situations. The safe and smooth trajectories in scenarios 1, 2 and 3 imply that this approach can be effectively used in real-life applications where multiple tasks are to be performed synchronously, asynchronously or both.

9. Discussion

LbCS has been utilized in this research to guide qAMM's car-like base and its revolute arms to designated targets. The proposed technique provides solutions for

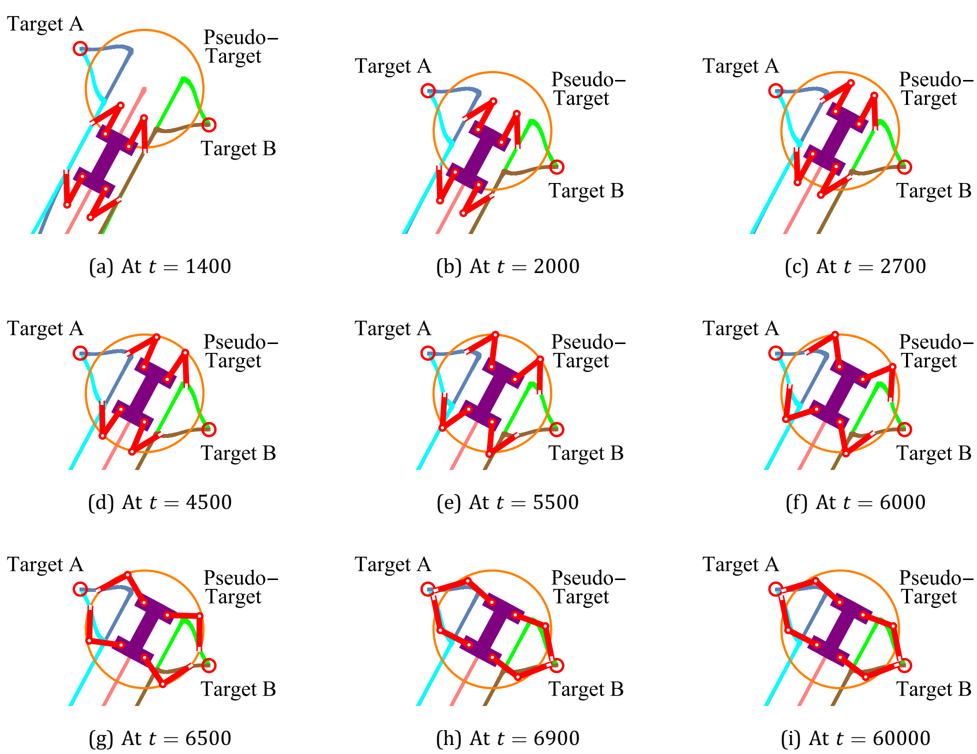

Fig. 9. Snapshots showing qAMM approaching its pseudo-target and end-effector targets A and B. The trajectory colors are same as stated in Fig. 8(b) and qAMM's path is same as shown in Fig. 8(a). The orientation and position of qAMM at $t = 1400, 2000, 2700, 4500, 5500, 6000, 6500, 6900$ and 60000, respectively, show that the left and right arms converge to their assigned targets simultaneously in synchronous motion as desired.

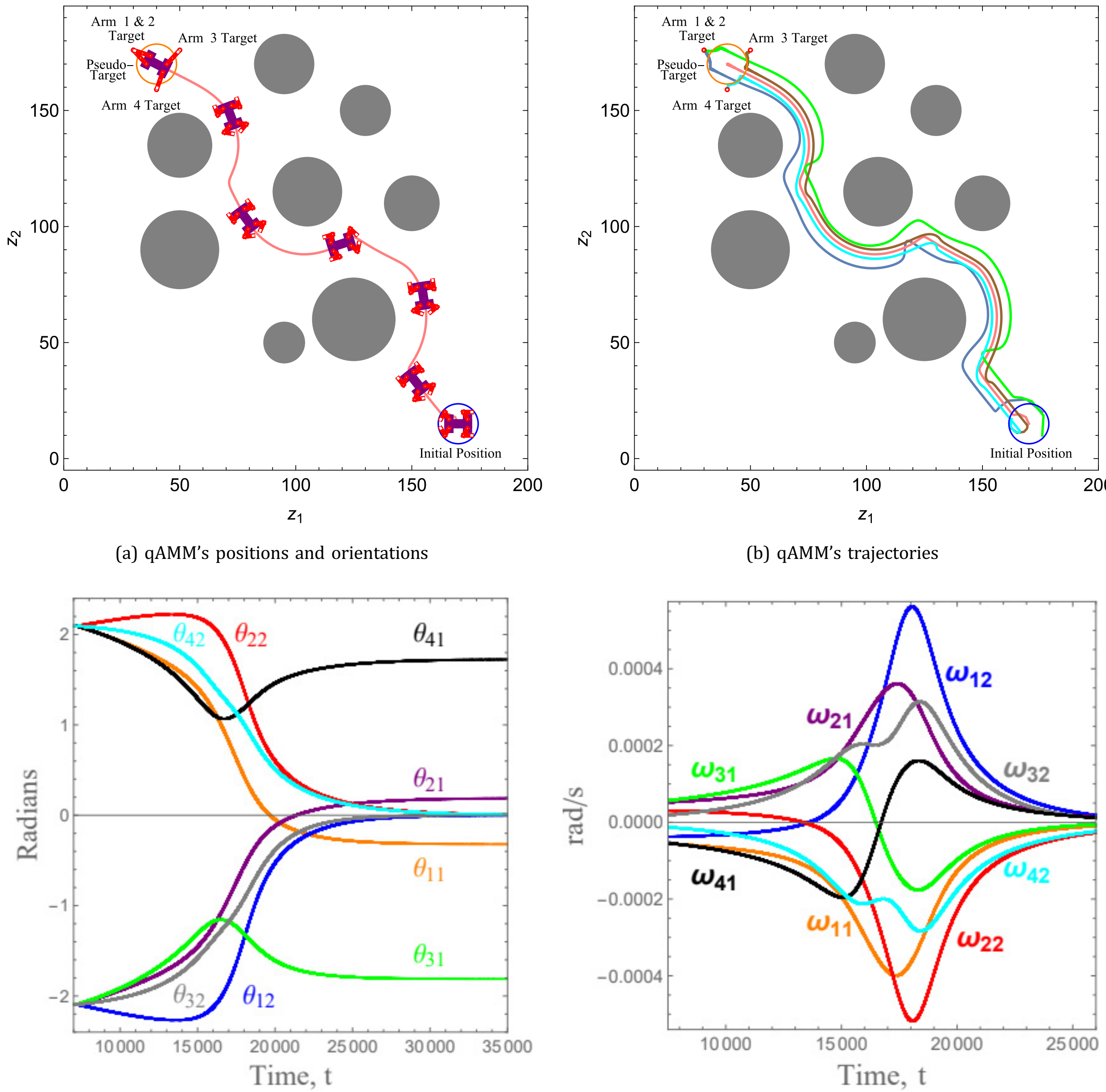

(a) qAMM's positions and orientations

(b) qAMM's trajectories

(c) Revolute link orientations

(d) Revolute link angular velocities

Fig. 10. (a) qAMM's positions at times $t = 1, 100, 500, 1000, 1600, 2500$ and 40000. (b) The car-like vehicle's trajectory is traced in pink, while that of arms $1, 2, 3$ and 4 are traced in thistle, green, brown, and cyan, respectively. (c) Orientations of qAMM's revolute links. (d) Angular velocities of qAMM's revolute links.

performing complex, tiresome, and multiple repetitious tasks. Apart from the controllers' effectiveness in producing smooth motion for navigation in obstacle-ridden environments, the additional feature of performing tasks synchronously and asynchronously guarantees that qAMM provides an ideal solution to autonomously carry out operations requiring multiple tasks, such as rubbish collection, cleaning, maintenance, and assembly of parts simultaneously.

As depicted by the results in Sec. 10, qAMM, as a single robot, can perform multiple tasks with the synchronous and asynchronous motion of its arms that could have otherwise required numerous robots as shown in [18]. For multi-tasking operations, the mobile manipulator proposed in this research is a better, more comprehensive, and cost-effective option than the cooperative dual-arm manipulators utilized in [22] or the multiple robots used in [18], as LbCS controllers offer continuous control compared to the

Table 4. Numerical values of parameters used in Scenario 3.

Dimensions	
$L \times L_1$	8×4
$\epsilon_1 = \epsilon_2$	3
l_{ij}	3.5
Initial configurations	
(x_{c_0}, y_{c_0})	(170,15)
θ_{ij_0}	$\theta_{11_0} = \theta_{22_0} = \theta_{41_0} = \theta_{42_0} = \frac{2\pi}{3}$, $\theta_{12_0} = \theta_{21_0} = \theta_{31_0} = \theta_{32_0} = \frac{-2\pi}{3}$
Control parameters	
$\eta_1 = \eta_2$	900
η_{i+2}	2
γ_q	6
Obstacles and targets	
k	8
(a_c, b_c)	(40,170)
(a_i, b_i)	Arm 1 and 2 Target= $(a_1, b_1) = (a_2, b_2) = (30, 176)$, Arm 3 Target $= (a_3, b_3) = (50, 176)$, Arm 4 Target $= (a_4, b_4) = (40, 159)$

noncontinuous, heuristic search-based controllers of [22] and the feedback delays encountered in [18]. Furthermore, for specific single tasks like picking up heavy objects that require cooperation and coordination from numerous robots, qAMM can perform such a task single-handedly, enabled by synchronous coordination of its four arms, as demonstrated in Figs. 8(a) and 10(a).

Synchronized and asynchronized robotic arm mobile manipulators have a promising future in carrying out multiple tasks in modern industrial and smart city environments. Therefore, it is feasible to include the approach presented in this research in specific applications of industrial and smart city environments that require multiple tasks to be performed effectively and efficiently.

Limitations

(1) In this study, the authors have restricted themselves to showing the effectiveness of acceleration-based control laws using numerical proofs and computer-based simulations of interesting scenarios. This paper provides a theoretical exposition into the applicability of LbCS only wherein the kinematic equations governing qAMM are considered in a constrained dynamic environment, and the acceleration-based control laws achieved were not integrated into some prototype experimental robots for practical results.
(2) The Lyapunov-based acceleration controllers can lead to local minima, causing the arms to converge and get stuck into undesired equilibrium points. However, the likelihood of getting stuck in undesired equilibria can be reduced by carefully selecting initial conditions and the control parameters using the brute-force technique.

10. Conclusion

Including additional robotic arms can significantly improve a mobile manipulator's effectiveness in performing multiple tasks by providing greater control over its environment. A theoretical exposition of a quad-arm car-like mobile manipulator's design, modeling, and motion control using stabilizing two-dimensional switched acceleration-based controllers was proposed in this research. LbCS was used to derive continuous time-invariant acceleration-based control laws to solve the mobile manipulator's navigation in performing multiple operations in an obstacle-ridden environment. The nonlinear switched controllers enabled qAMM to navigate from an initial configuration to assigned pseudo-target and target locations while avoiding obstacles and observing the system restrictions and limitations. Moreover, the acceleration-based motion controllers guaranteed smooth trajectories for qAMM while performing tasks synchronously and asynchronously, as required. From the authors' perspective, this is the first time such continuous switched acceleration-based controllers are derived for a four-arm mobile system in Lyapunov's sense.

The direct benefit of such autonomous mobile robot technology to smart city operations is significantly increased performance and multi-tasking capability for use as intelligent vehicle systems. The proposed mobile manipulator is highly suitable for various multi-tasking operations in relevant smart city sectors, such as waste management, garbage collection, construction, cleaning, and maintenance. In future work, combining the current algorithm with artificial intelligence (AI) methods and experimental prototype robots will be considered for a car-like mobile manipulator that performs multiple tasks while addressing the limitation of the LbCS approach. Moreover, connectivity maintenance constraints for the arms in conjunction with inter-arm collision avoidance will be explored to enhance the functionality and efficiency of qAMM.

ORCID

Ravinesh Chand https://orcid.org/0000-0003-2861-3039
Sandeep A. Kumar https://orcid.org/0000-0002-6951-4742
Bibhya Sharma https://orcid.org/0000-0002-7519-7712
Ronal P. Chand https://orcid.org/0000-0002-8527-040X

References

[1] N. Kousi, G. Michalos, S. Aivaliotis and S. Makris, An outlook on future assembly systems introducing robotic mobile dual arm workers, *Procedia CIRP* **72** (2018) 33–38.

[2] B. Esmaeilian, B. Wang, K. Lewis, F. Duarte, C. Ratti and S. Behdad, The future of waste management in smart and sustainable cities: A review and concept paper, *Waste Manag.* **81** (2018) 177–195.

[3] M. H. Abbasi, B. Majidi and M. T. Manzuri, Deep cross altitude visual interpretation for service robotic agents in smart city, *2018 6th Iranian Joint Congress on Fuzzy and Intelligent Systems (CFIS)* (IEEE, 2018), pp. 79–82.

[4] B. Sharma, S. Singh, J. Vanualailai and A. Prasad, Globally rigid formation of *n*-link doubly nonholonomic mobile manipulators, *Robot. Auton. Syst.* **105** (2018) 69–84.

[5] A. Prasad, B. Sharma, J. Vanualailai and S. Kumar, Motion control of an articulated mobile manipulator in 3D using the Lyapunov-based control scheme, *Int. J. Control* **95** (2021) 2581–2595.

[6] N. I. Bouaziz, O. Mechali, K. L. Besseghieur and N. Achour, Trajectory planning for autonomous formation of wheeled mobile robots via modified artificial potential field and improved PSO algorithm, *Unmanned Syst.* **12** (2024) 1085–1104.

[7] R. Chand, S. A. Kumar, R. P. Chand and S. Reddy, A car-like mobile manipulator with an *n*-link prismatic arm, *2021 IEEE Asia-Pacific Conf. Computer Science and Data Engineering (CSDE)* (IEEE, 2021), pp. 1–6.

[8] S. Angerer, C. Strassmair, M. Staehr, M. Roettenbacher and N. M. Robertson, Give me a hand-the potential of mobile assistive robots in automotive logistics and assembly applications, *2012 IEEE Int. Conf. Technologies for Practical Robot Applications (TePRA)* (IEEE, 2012), pp. 111–116.

[9] S. Byrne, W. Naeem and S. Ferguson, Improved APF strategies for dual-arm local motion planning, *Trans. Inst. Meas. Control* **37**(1) (2015) 73–90.

[10] C. Smith, Y. Karayiannidis, L. Nalpantidis, X. Gratal, P. Qi, D. V. Dimarogonas and D. Kragic, Dual arm manipulation - A survey, *Robot. Auton. Syst.* **60**(10) (2012) 1340–1353.

[11] S. K. Agrawal and S. Shirumalla, Planning motions of a dual-arm free-floating manipulator keeping the base inertially fixed, *Mech. Mach. Theory* **30**(1) (1995) 59–70.

[12] A. Atyabi and D. Powers, Review of classical and heuristic-based navigation and path planning approaches, *Int. J. Adv. Comput. Technol. (IJACT)* **5** (2013) 14.

[13] S. S. M. Salehian, N. Figueroa and A. Billard, Coordinated multi-arm motion planning: Reaching for moving objects in the face of uncertainty, in *Proc. Robotics: Science and Systems*, Ann Arbor, MI, USA, 2016.

[14] H. Seraji, A unified approach to motion control of mobile manipulators, *Int. J. Robot. Res.* **17**(2) (1998) 107–118.

[15] B. Sharma, J. Vanualailai and S. Singh, Lyapunov-based nonlinear controllers for obstacle avoidance with a planar *n*-link doubly nonholonomic manipulator, *Robot. Auton. Syst.* **60**(12) (2012) 1484–1497.

[16] X. Lin, Y.-J. Yu, S.-Z. Chen and Y.-Y. Shi, An improved apf method for complex and dynamic obstacles avoidance, *Unmanned Syst.* **11**(02) (2023) 175–189.

[17] J. Vanualailai, B. Sharma and S.-i. Nakagiri, An asymptotically stable collision-avoidance system, *Int. J. Non-Linear Mech.* **43**(9) (2008) 925–932.

[18] H. Eberle, S. Nasuto and Y. Hayashi, Synchronization-based control for a collaborative robot, *R. Soc. Open Sci.* **7**(12) (2020) 201267.

[19] T. Takahama, K. Nagatani and Y. Tanaka, Motion planning for dual-arm mobile manipulator-realization of "tidying a room motion", *IEEE Int. Conf. Robotics and Automation, 2004. Proc. ICRA'04. 2004*, Vol. 5 (IEEE, 2004), pp. 4338–4343.

[20] C. West, F. Arvin, W. Cheah, A. West, S. Watson, M. Giuliani and B. Lennox, A debris clearance robot for extreme environments, *Annual Conf. Towards Autonomous Robotic Systems* (Springer, 2019), pp. 148–159.

[21] M. J. C. Samonte, S. H. Baloloy and C. K. J. Datinguinoo, e-TapOn: Solar-powered smart bin with path-based robotic garbage collector, *2021 IEEE 8th Int. Conf. Industrial Engineering and Applications (ICIEA)* (IEEE, 2021), pp. 181–185.

[22] X. Chen and J. He, Cooperative planning of dual arm robot based on improved particle swarm optimization, *2021 IEEE 3rd Int. Conf. Civil Aviation Safety and Information Technology (ICCASIT)* (IEEE, 2021), pp. 632–635.

[23] C. Cohen and D. Rouhling, A formal proof in Coq of LaSalle's invariance principle, *Int. Conf. Interactive Theorem Proving* (Springer, 2017), pp. 148–163.

[24] J. LaSalle, Some extensions of Liapunov's second method, *IRE Trans. Circuit Theory* **7**(4) (1960) 520–527.

[25] S. A. Kumar, B. Sharma, J. Vanualailai and A. Prasad, Stable switched controllers for a swarm of UGVs for hierarchal landmark navigation, *Swarm Evol. Comput.* **65** (2021) 100926.

Ravinesh Chand received his Postgraduate Diploma and Master of Science in Applied Mathematics from The University of the South Pacific (USP) in 2014 and 2019, respectively. He is pursuing the Doctor of Philosophy in Applied Mathematics program at USP. He is currently serving as a Lecturer in Mathematics at the Fiji National University (FNU) in Suva, Fiji. His research interests include robotic manipulation, control theory, modeling and simulation of robotic systems, path planning and motion control of autonomous systems.

Sandeep A. Kumar received his M.Sc. and Ph.D. degrees from the University of the South Pacific (USP) in 2014 and 2024, respectively. Currently, he is serving USP as an Assistant Lecturer in Mathematics. His research focuses on motion planning and control in robotics, inspired by nature. He designs nonlinear, time-invariant, continuous, stabilizing algorithms using the Lyapunov-based control scheme for complex mechanical systems in constrained environments. His work, primarily theoretical, has applications in autonomous assistive wheelchairs, UAV swarms for EEZ surveillance, and robotic manipulators. He is also investigating the applicability of other classical, heuristic, and hybrids which could provide better problem-based solutions in his research areas.

Bibhya Sharma is a Professor of Mathematics and the Head of School of School of Information Technology, Engineering, Mathematics and Physics at USP. He also served as Associate Dean for Learning and Teaching within the Faculty of Science, Technology and Environment at USP from 2010–2019. He is a member of several professional mathematics societies and unions and has published more than 100 articles and book chapters in the fields of mathematics education, robotics, biologically inspired processes and the TLPs of higher education.

Ronal P. Chand is a Lecturer in Mathematics at Fiji National University. He holds a Postgraduate Diploma and a Master of Science in Mathematics. Currently, he is pursuing Ph.D. in Mathematics from Fiji National University. His research focuses on developing algorithms and mathematical models for motion control and planning for robotic systems.